

Reviewer 1

General comments:

This study makes an extensive and comprehensive national distribution of the aerosol optical properties and direct radiative effect during 2008-2017 in China over decade change. The aerosol key optical parameter obtained from CARSNET, and this ground-based observation net was established independently with Chinese characteristics. The instrument calibration and inversion algorithm from CARSNET has been recognized by the international community, and the results have also been compared by the global ground based observational organizations such as AERONET, etc. Generally, five regions including 50 ground stations nationwide were defined in this study, covers almost the whole region of China, which is of great research value contributed to the regional aerosol optical properties in China, East Asia or the whole world. An emphasis on the estimation of the aerosol optical properties over China vast and varied terrain under different background and aerosol sources driven by the meteorological factors and climatology changes have been employed. The objective of the paper is challenging to use the National scale, ground-based measurements of aerosol microphysical and its optical properties as well as direct radiative effect obtained from the sunphotometer with good quality and large databases. The paper is well written with most importance to complement and support the climatology for aerosol microphysical and optical properties of China and provide better understanding of the aerosols' climate effects over the different types of sites covering a broad expanse of China. Thus, I would suggest a minor revision before it is considered for publication as following.

Response: Thanks for the reviewer's important comments; some important revisions and the grammar have been corrected according to the reviewer's suggestions.

Special comments:

1. Line 40, the time period for the data at the observation site need a brief description in the Abstract.

Response: Thanks for the suggestions. The time period for the data at the observation site has been briefly described as "Multi-year observations of ..." in the Abstract.

2. Line 60-61, the word “useful” could be changed as “important” to avoid repetition.

Response: The word “useful” has been changed as “important” to avoid repetition in the manuscript.

3. Line 95-96, some references could be added there.

Response: Following the suggestion of reviewer, some references have been added in the revised paper as “...in many regions of China (Che et al., 2009c, 2018; Zhao et al., 2018)”.

4. Line 126-127, “aerosol size distribution” could be changed as “aerosol size distribution (volume and aerosol effective radii)”.

Response: The words “aerosol size distribution” has been changed as “aerosol size distribution (volume and aerosol effective radii)” in the revised manuscript.

5. Line 196, “Ångström” should be changed as “Ångström exponent” to make consistency in the text.

Response: Thank for the suggestions of reviewers. The words “Ångström” has been changed as “Ångström” and this change applied to the rest of the manuscript.

6. Line 271, “...was found to be substantially...” should be better revised as “...was found substantially...”.

Response: According the reviewer’s suggestions, the words “...was found to be substantially...” has been modified as “...was found substantially...”.

7. Line 297, “...also was high, 0.30 $\mu\text{m}^3/\mu\text{m}^2$.” should be better revised as “...also was high to 0.30 $\mu\text{m}^3/\mu\text{m}^2$.”.

Response: Thanks for the suggestion. The words “...also was high, 0.30 $\mu\text{m}^3/\mu\text{m}^2$.” has been modified in the revised manuscript as “...also was high to 0.30 $\mu\text{m}^3/\mu\text{m}^2$.”.

8. Line 331-332, please specify the results of Zhao et al. (2018) in detail.

Response: Follow up on the reviewer’s suggestion, the sentences has been changed as “Zhao

et al. (2018) also reported the effect of sea salt aerosol on the aerosol absorption and radiative effects in the coastal region over northeastern China.” in the revised manuscript.

9. Line 375, “...in and around...” should be better revised as “...in or around...”.

Response: Done. The words of “...in and around...” was changed as “...in or around...” in the revised paper.

10. Line 432, “...these particles originate from a multitude of sources...” should be better revised as “...these particles originate from multitude sources...”.

Response: The sentence “...these particles originate from a multitude of sources...” has been changed as “...these particles originate from multitude sources...”.

11. Line 437, “were more than likely” should be better revised as “were more likely”.

Response: The words “were more than likely” have been changed as “were more likely” in section 3.3.

12. Line 442, “(EAE 0.25)” should be better revised as “(EAE = 0.25)”.

Response: The words “(EAE 0.25)” has been changed as “(EAE = 0.25)” in the revised version.

13. Line 474, “...the aerosol was more absorbing in fall, ...” should be better revised as “...the aerosol was more absorbing in autumn, ...”.

Response: The words “...the aerosol was more absorbing in fall, ...” has been changed as “...the aerosol was more absorbing in autumn, ...”, and this change applied to the rest of the manuscript.

14. Line 482-483, “Therefore, the different SSA440nm distributions in the two regions may be attributed by the special aerosol composition.” Is the special aerosol composition because of the industrial structure of different regions Like the Northeastern China was once the significant heavy industries base in China.

Response: According to the suggestion, the sentences “Therefore, the different SSA440nm distributions in the two regions may be attributed by the special aerosol composition” has been changed as “Therefore, the different SSA440nm distributions in the two regions may be attributed by the special aerosol composition related to the urban-industrial background of northeastern China (lower SSA440nm) and more anthropogenic sources in the eastern China environmental (higher SSA440nm).” in the revised manuscript.

15. Line 542, “aerosol direct radiative effect” in the section title should be better revised as “direct aerosol radiative effect”.

Response: Thanks for the suggestions. The title of the section 3.5 has been changed as “direct aerosol radiative effect” to consistent with the rest of revised manuscript.

16. Line 554, “-22.13 and -17.43” should be better revised as “-22.13 and -17.43 W/m²”.

Response: According to the suggestion, the “-22.13 and -17.43” has been changed as “-22.13 and -17.43 W/m²” in the revised manuscript.

17. Line 583, “A notably small” should be better revised as “A notably small positive”.

Response: Thanks for the reviewer’s suggestions. We checked the value of DARE-TOA in Akedala carefully, and found that it should be corrected as -0.42 W/m² in the text by a typing mistake. Moreover, the value was correct in the relevant descriptive sentences, Table and charts through the text.

18. Line 588, “(SSA 0.92)” should be better revised as “(SSA = 0.92)”.

Response: Done. The words “(SSA 0.92)” has been changed as “(SSA = 0.92)”.

19. Line 607, “as” should be deleted.

Response: The word “as” have been deleted in the revised paper.

Reviewer 2

General comments

This paper characterizes the climatology of aerosol microphysical and optical properties in China using ground-based remote sensing from the CARSNET network. This is one of the most systematic dataset of aerosol optical properties reported in the literature, and is valuable for improving the estimate of aerosol radiative effects and for evaluation of satellite data and climate models. The paper is generally well written. I think it can be considered for publication after the author addresses the following minor comments and suggestions. Besides the following comments, however, there are many outstanding grammar errors in the paper. I strongly suggest that the author ask a native speaker to carefully edit and improve the language.

Response: Thanks for the reviewer's important and constructive comments and suggestions. Some minor comments and suggestions have been revised carefully in the manuscript. Moreover, the grammar has been carefully checked in the paper and the language of this manuscript has been improved by a native speaker.

Special comments:

(1) Line 72-77: The descriptions of the roles of AOD, absorptivity, and SSA are very similar. Please revise a bit to reflect their respective roles.

Response: According the reviewer's suggestions, the descriptions of the roles of AOD, absorptivity, and SSA has been modified to reflect their roles, respectively. The text is as follows:

"Aerosol optical depth (AOD) is one of the key measures of the total aerosol extinction effects on climate (Breon et al., 2002), and the extinction Ångström exponent (EAE) with spectral dependence can be used to obtain the information about aerosol size distributions (Gobbi et al., 2007; Eck et al., 1999; Zheng et al., 2017). The aerosols' absorptivity depends on particle composition is a key determinant to calculate the direct aerosol radiative effect (Haywood and Shine, 1995; Li et al., 2016; Zheng et al., 2018), and the single scattering albedo (SSA) is the parameter has spectral dependence to distinguish major aerosol particle types (Jacobson et al., 2000; Dubovik et al., 2002; Gelencser et al., 2004; Russell et al., 2010;

Giles et al., 2012).”.

(2) Line 241-243: Which radiative transfer model is used to calculate the direct aerosol radiative effect?

Response: Following the reviewer’s suggestions, the radiative transfer model of Discrete Ordinates (DISORT) approach was used to calculate the direct aerosol radiative effect which has been described in the manuscript.

(3) Line 258-259: The assumption of single fixed aerosol vertical distribution (exponential to 1 km) may deviate from the real-world situation significantly. What’s the potential impact on calculated aerosol radiative effect?

Response: Thank for the reviewer’s comments. Firstly, according to the Zhao et al. (2019, AE) pointed out that the distribution of annual MLH in the most land regions of China were less than 1km. Aerosols are mainly distributed within the mixing layer in the atmosphere and usually decrease with the increase of mixing layer height. Therefore, this paper assumes 1 km to calculate the radiation flux is reliable and reasonable. In addition, the single fixed aerosol vertical distribution (exponential to 1 km) assumed in this study were to be consistent with other previous researches in the world, which also adopted this standard.

(4) Line 260-262: What does this error refer to and how is it quantified?

Response: Thank for the suggestions of reviewer. “The error for the observed solar radiation at the surface in global was $+2.1 \pm 3.0\%$ for an overestimation of about $+9 \pm 12 \text{ Wm}^{-2}$.” was refer to García et al. (2008). The text has been modified as “García et al. (2008) pointed out that the error for the observed solar radiation at the surface in global was $+2.1 \pm 3.0\%$ for an overestimation of about $+9 \pm 12 \text{ Wm}^{-2}$.”.

Moreover, García et al. (2008) found that a small overestimation of $9 \pm 12 \text{ Wm}^{-2}$ for measured radiation in global terms within the uncertainty of solar measurements by BSRN (Baseline Surface Radiation) and SolRad-Net (Solar Radiation Networks) observed data.

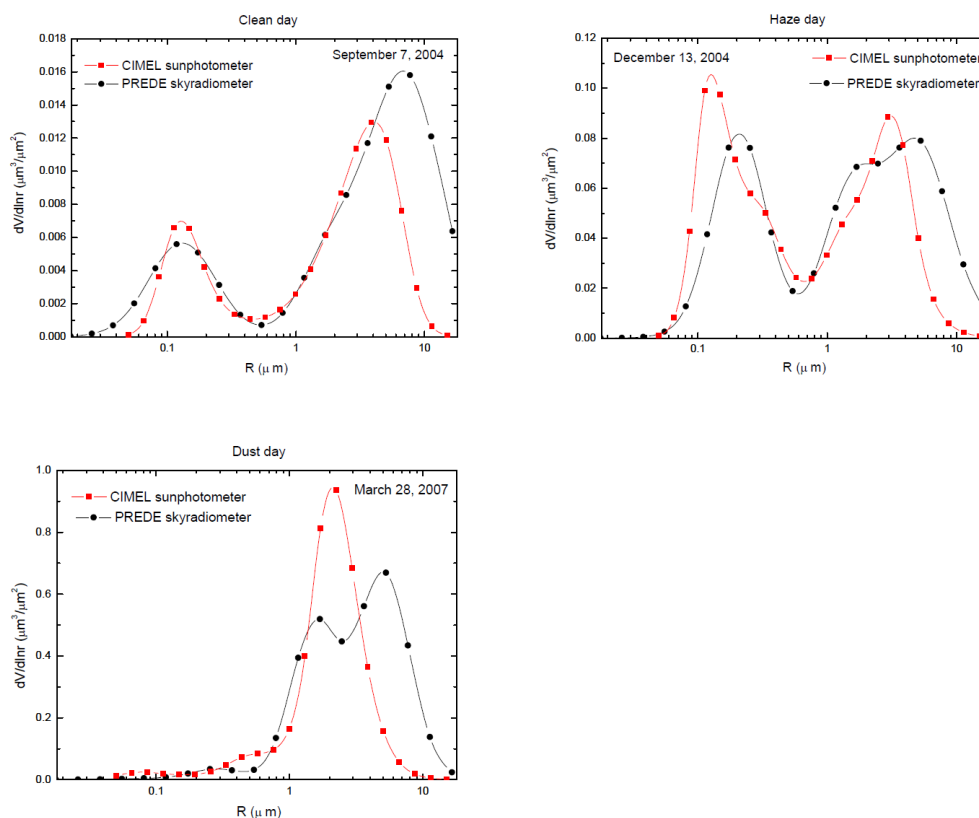
(5) Line 285-287: PVF and PVC have been defined before (Line 216) and the full names used

in these two places are different. Please define only once and use consistent terms.

Response: Thanks for the suggestions. The “PV_F” and “PV_C” have been defined as “PV_F” and “PV_C” to make consistent throughout the text in the revised paper.

(6) Line 314-316: In urban sites, the volume concentration of coarse particles is higher than fine particles, which sounds counterintuitive. Does this agree with previous studies?

Response: The authors agree with the reviewer’s opinion. Firstly, the volume concentration of fine particles is higher than that of the coarse particles at most of the pollution period; but during the non-pollution period, the volume concentration of coarse particles is higher than fine particles. Che et al. (2008, ACP) has investigated that the volume concentration of coarse particles is higher than fine particles in the clean day as can be seen in the figure below. The results of this manuscript are a multi-year average and agree with previous studies. Moreover, Zhao et al. (2018, JGR) has also found the larger volume concentration of coarse mode particles than fine mode particles in the industrial-urban site of Fushun in Northeastern China. Finally, in these 23 urban sites of this study, there are almost 15 cities in Northern China, where have less precipitation and higher fugitive dust contribution level. These climatic conditions could lead to the higher volume concentration of coarse particles in such urban sites.



(7) Line 334-335: The several studies listed here did not support the hygroscopic growth of fine-mode particles.

Response: Thanks for the reviewer's comments. More references have been added to supplement the hygroscopic growth of fine-mode particles in the revised version. The text is as follows:

“Cheng et al. (2015) found different aerosol volume size distributions for dust and sea salt at Shanghai in the eastern China, and they showed that their relative abundances varied with season and in response to local or long-range transport. Zhao et al. (2018) also reported the effect of sea salt aerosol on the aerosol absorption and radiative effects in the coastal region over northeastern China. Especially the particles hygroscopic growth with different composition observed in special climatic conditions could affect aerosol microphysical properties by geographically variable effects (Zhang et al., 2015; Sun et al., 2010). Like in the YRD region, hygroscopic growth of fine-mode particles could lead to larger AOD and scattering enhancing reported by Sun et al. (2018) and Che et al. (2018). Xia et al. (2019) observed the aerosol hygroscopic growth on fine particle scattering coefficient in Beijing.”.

Moreover, some references has been added as following:

Sun, J. Y., Zhang, Q., Canagaratna, M. R., Zhang, Y. M., Ng, N. L., Sun, Y. L., Jayne, J. T., Zhang, X. C., Zhang, X. Y., and Worsnop, D. R.: Highly time- and size-resolved characterization of submicron aerosol particles in Beijing using an Aerodyne Aerosol Mass Spectrometer, *Atmos. Environ.*, 44, 131-140, 2010.

Sun, T., Che, H., Qi, B., Wang, Y., Dong, Y., Xia, X., Wang, H., Gui, K., Zheng, Y., Zhao, H., Ma, Q., Du, R., and Zhang, X.: Aerosol optical characteristics and their vertical distributions under enhanced haze pollution events: effect of the regional transport of different aerosol types over eastern China, *Atmos. Chem. Phys.*, 18, 2949–2971, <https://doi.org/10.5194/acp-18-2949-2018>, 2018.

Xia, C., Sun, J. Y., Qi, X. F., Shen, X. J., Zhong, J. T., Zhang, X. Y., Wang, Y. Q., Zhang, Y. M., and Hu, X. Y.: Observational study of aerosol hygroscopic growth on scattering coefficient in Beijing: A case study in March of 2018, *Sci. Total Environ.*, 685, 239-247, 2019.

Zhang, L., Sun, J. Y., Shen, X. J., Zhang, Y. M., Che, H., Ma, Q. L., Zhang, Y. W., Zhang, X. Y., and Ogren, J. A.: Observations of relative humidity effects on aerosol light scattering in the Yangtze River Delta of China, *Atmos. Chem. Phys.*, 15, 8439-8454, <https://doi.org/10.5194/acp-15-8439-2015>, 2015.

(8) Line 369, Line 577: Wuhan is not located in the YRD region.

Response: According to the reviewer's suggestion, the location of Wuhan has been checked and modified to central China all through the text.

(9) Line 583-585: Why is the DARE-TOA positive in Akedala? Due to a strong absorption?

Response: Thanks for the important suggestions. We checked the value of DARE-TOA in Akedala, it should be corrected as -0.42 W/m² in the text by a typing mistake. Moreover, the value was correct in the relevant descriptive sentences, Table and charts through the text.

(10) Line 610-612: I think the strong cooling is not due to strong absorption.

Response: According to the reviewer's helpful suggestion, the sentences "The high DARE-TOA values at these urban sites imply relatively strong cooling effects due to moderate to strong light absorption by the particles." has been revised as "The high DARE-TOA values at these urban sites imply relatively strong cooling effects due to higher aerosol loadings in the atmosphere."

(11) Fig. 2, 3, 8: The scales of the legend should be modified to differentiate large and small values more clearly. For example, in Fig. 8, most values fall between -40 and 0 and hence show the same color.

Response: Thanks for the suggestions. The legend scales of Figure 2 - 8 have been changed in the revised manuscript to differentiate large and small values more clearly as follows:

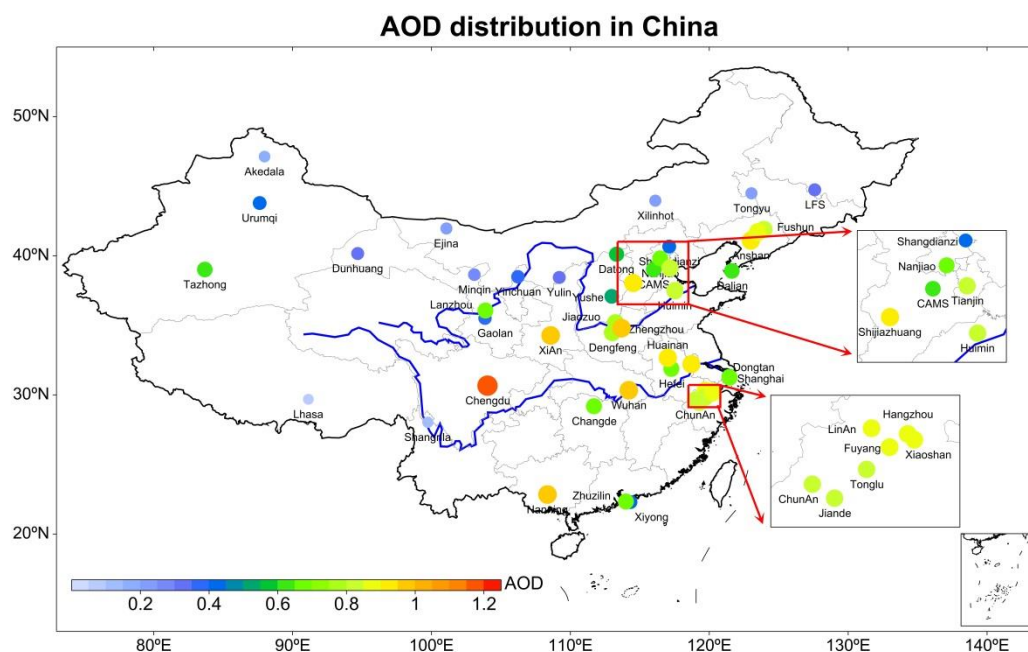


Figure 2. Annual spatial distribution of aerosol optical depth (AOD) at 440 nm at the CARSNET sites

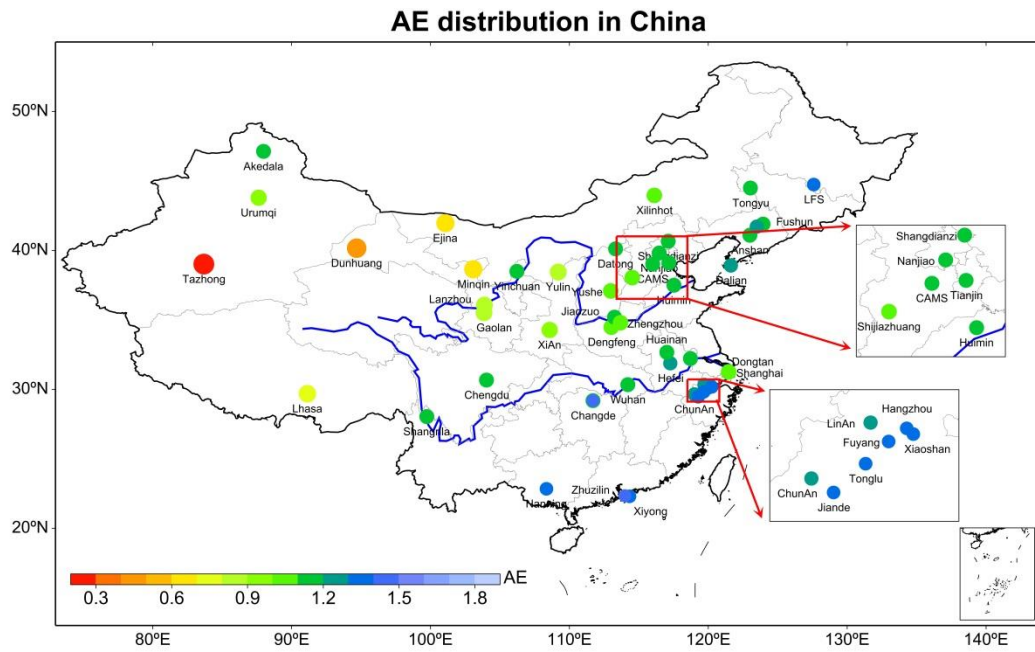


Figure 3. Annual spatial distribution of extinction Ångström exponent (AE) 440-870 nm at the CARSNET sites

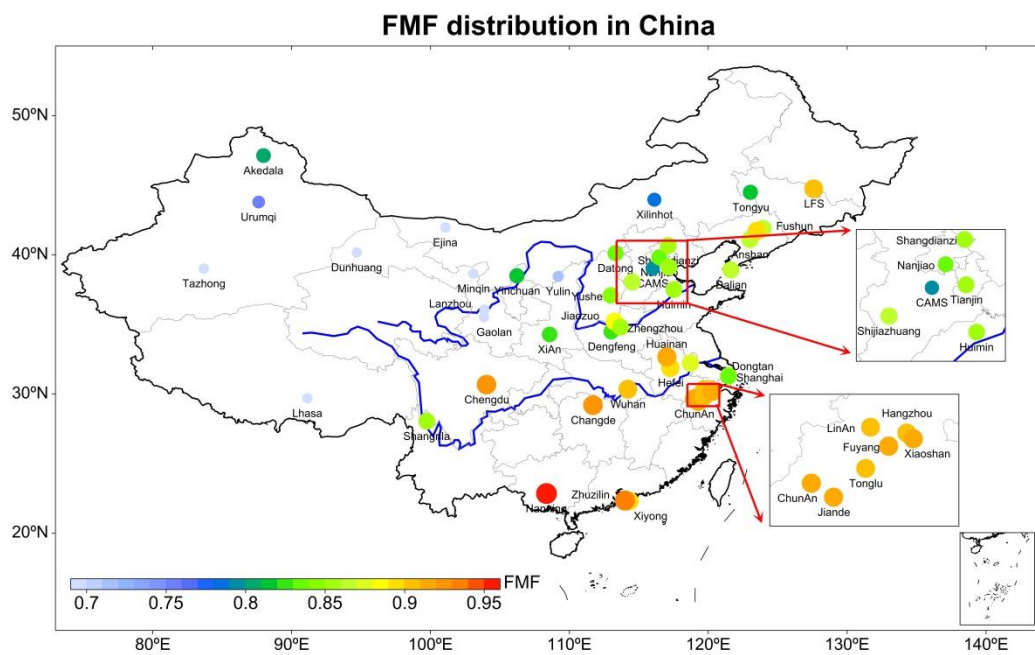


Figure 4. Annual spatial distribution of fine mode fraction at the CARSNET sites

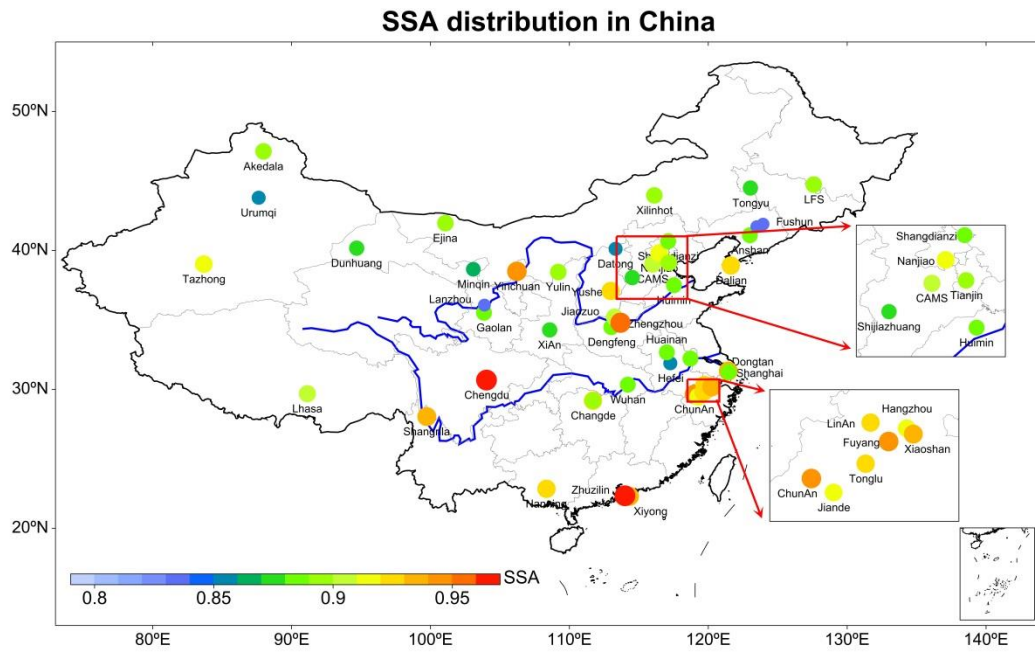


Figure 5. Annual spatial distribution of the single scattering albedo (SSA) at 440 nm at the CARSNET sites

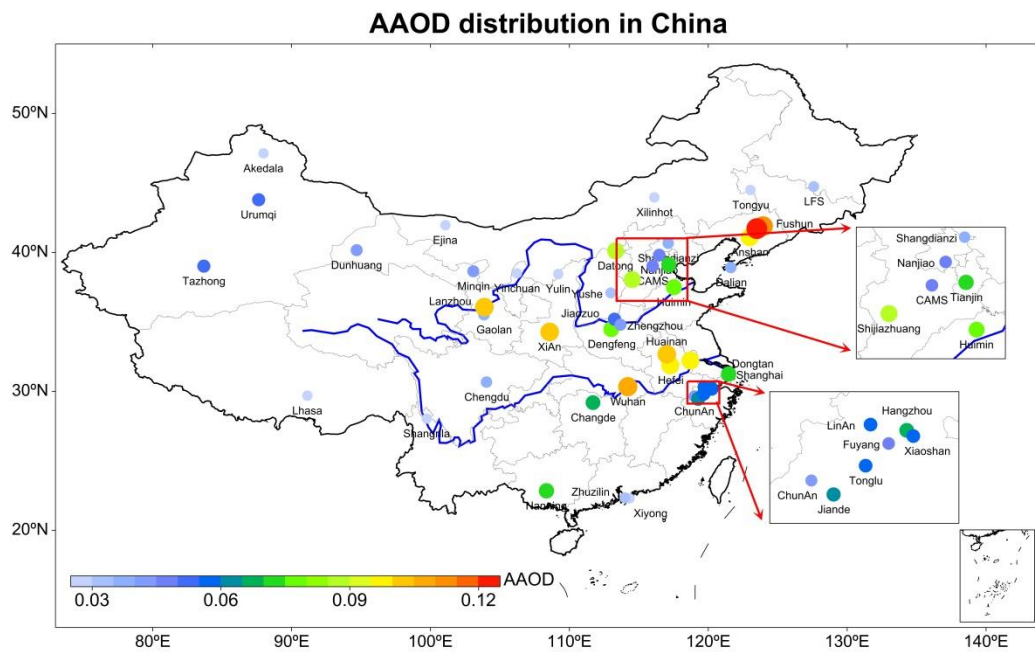


Figure 6. Annual spatial distribution of absorption aerosol optical depth (AAOD) at 440 nm at the CARSNET sites

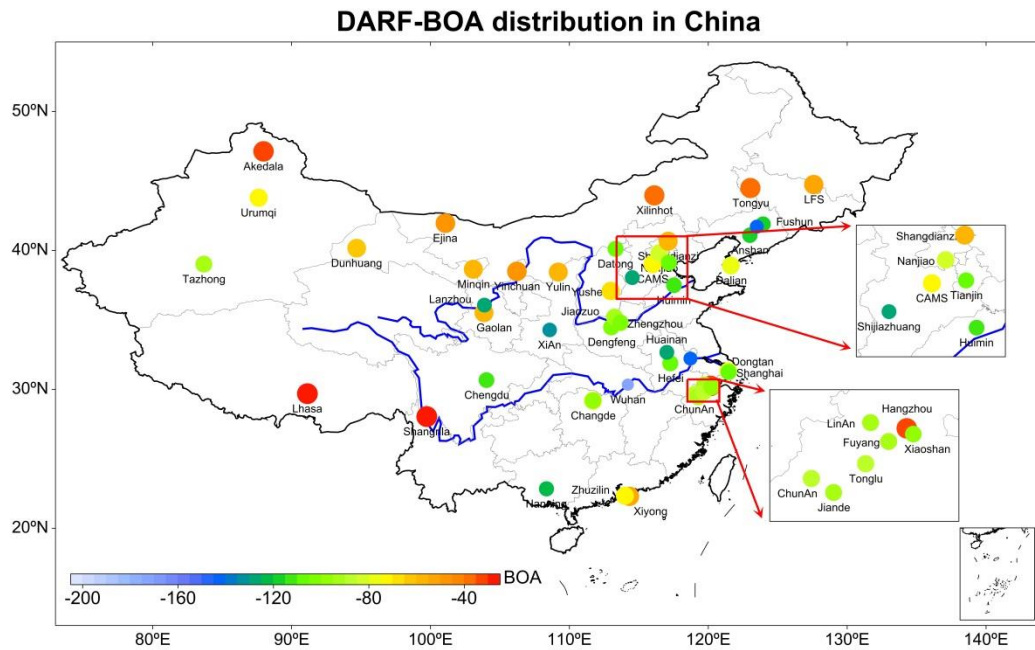


Figure 7. Annual spatial distribution of direct aerosol radiative effect at the bottom of the atmosphere at the CARSNET sites

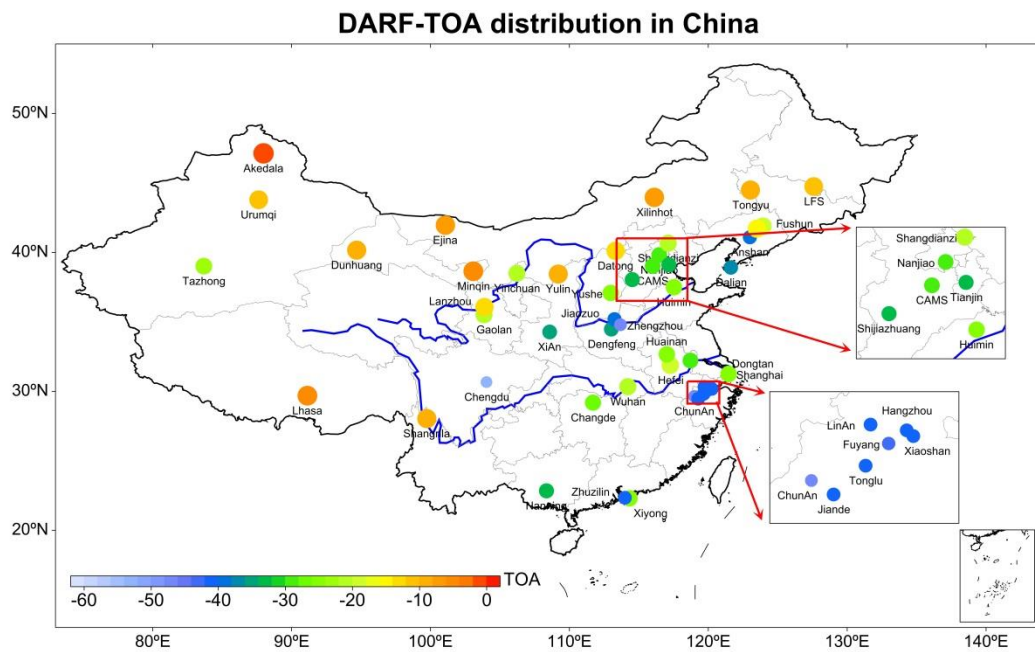


Figure 8. Annual spatial distribution of direct aerosol radiative effect at the top of the atmosphere at the CARSNET sites

Reviewer 3

General comments:

Che et al. "Spatial distribution of aerosol microphysical and optical properties and direct radiative effect from the China Aerosol Remote Sensing Network" This study takes the advantage of the multi-band original observation data of the sunphotometer for many years from the China Aerosol Remote Sensing Network, and applies ground inversion method to calculate the atmospheric aerosols optical characteristic parameters. The authors sorted and processed the data results in aerosol optical properties in China. The results of this study established a ground aerosol remote sensing optical parameters dataset which is more complete, accurate and reliable in China. This work will help to improve China's climate change research and even for the East Asia. This research enhanced the understanding of aerosol optical properties in different regions of China. I would suggest its publication after minor revision.

Response: We thank for the reviewer's comments and suggestions. The manuscript has been revised in some minor changes.

Special comments:

1. Lines 67-69. It is well known that the aerosol-cloud interaction plays very important roles to the radiation balance and remains as the largest uncertainty in climate model prediction, even more important than the aerosol direct radiative effect. Before diving into aerosol direct effect, one or two sentences of description about the aerosol indirect effects might be necessary. For example, Garrett and Zhao (2006, DOI: 10.1038/nature04636) and Zhao and Garrett (2015, doi:10.1002/2014GL062015) have shown the warming effect in longwave radiation by aerosol indirect effect in the Arctic, Xie et al. (2013, 10.1175/JCLI-D-12-00517.1) show the cooling effect of aerosol indirect effect. For aerosol direct radiative effect, Yang et al. (2016, doi:10.1002/2016JD024938) particularly indicate (also) the optical properties of aerosols determine the particle direct radiation effect.

Response: Thanks for the reviewer's suggestion. The authors agree with the reviewer's opinion that the aerosol indirect effects could be same important as the aerosol direct radiative effect such as the aerosol-cloud interaction which play very important roles to the radiation

balance. Some description about the aerosol indirect effects has been added in the revised paper. The text is as follows:

“Atmospheric aerosols have important direct effects on climate because they can scatter and absorb radiant energy and in so doing affect the Earth’s energy balance (Charlson et al., 1992; Yang et al., 2016). Meanwhile, the aerosols can be served as cloud condensation nuclei or ice nuclei to affect the climate indirectly through aerosol–cloud interactions (Twomey et al., 1984; Garrett et al., 2006; Zhao et al., 2015; Xie et al., 2013).”.

Moreover, the following references were now cited:

Garrett, T. J., and Zhao, C.: Increased Arctic cloud longwave emissivity associated with pollution from mid-latitudes, *Nature*, 440, 787–789, doi:10.1038/nature04636, 2006.

Xie, S., Liu, X., Zhao, C., and Zhang, Y.: Sensitivity of CAM5-Simulated Arctic Clouds and Radiation to Ice Nucleation Parameterization, *J. Climate.*, 26, 5981–5999, doi:10.1175/jcli-d-12-00517.1, 2013.

Yang, X., Zhao, C., Zhou, L., Wang, Y., and Liu, X.: Distinct impact of different types of aerosols on surface solar radiation in China, *J. Geophys. Res.-Atmospheres*, 121, 6459–6471. DOI: <https://doi.org/10.1002/2016jd024938>, 2016.

Zhao, C., and Garrett, T. J.: Effects of Arctic haze on surface cloud radiative forcing, *Geophys. Res. Lett.*, 42, 557–564. doi:10.1002/2014gl062015, 2015.

2. Lines 69-75, In addition to the climate impacts, aerosols also play important impacts on weather. For example, Zhao et al. (2018, doi: 10.1029/2018GL079427) showed that aerosol can enlarge the rainfall area of tropical cyclone, causing severe flooding damage.

Response: According to the helpful suggestions of reviewer, the text has been rewritten in the revised manuscript as follows:

“The optical properties of the aerosol determine the particles’ direct effects on the Earth’s radiative balance and weather-climate change (Ramanathan et al., 2001; Eck et al., 2005;

Myhre, 2009; Zhao et al., 2018).”

And the following reference was now cited:

Zhao, C., Lin, Y., Wu, F., Wang, Y., Li, Z., Rosenfeld, D., and Wang, Y.: Enlarging Rainfall Area of Tropical Cyclones by Atmospheric Aerosols, *Geophys. Res. Lett.*, doi:10.1029/2018gl079427, 2018.

3. Lines 73-75, Zheng et al. (2017, doi: 10.5194/acp-17-13473-2017) have done a comprehensive study about the aerosols based on AOD, size, angstrom exponent, PM2.5, and so on, which is worthy to mention here.

Response: Thanks for the suggestions of the reviewer. The comprehensive study of Zheng et al. (2017) about the AOD, size, angstrom exponent, PM2.5 has been added in the revised manuscript. The following reference was now cited:

Zheng, C., Zhao, C., Zhu, Y., Wang, Y., Shi, X., Wu, X., Chen, T., Wu, F., and Qiu, Y.: Analysis of influential factors for the relationship between PM2.5 and AOD in Beijing, *Atmos. Chem. Phys.*, 17, 13473–13489, doi: 10.5194/acp-17-13473-2017, 2017.

4. Lines 75-76, This is true. Actually, aerosol direct radiative effect can also be used to derive the absorptivity of aerosols. Some recent references might be worthy to be cited.

Response: According the reviewer’s suggestions, some recent references have been added in the revised paper and the text is as follows:

“The aerosols’ absorptivity depends on particle composition is a key determinant to calculate the direct aerosol radiative effect (Haywood and Shine, 1995; Li et al., 2016; Zheng et al., 2018), ...”

The following reference was now cited:

Zheng, Y., Che, H., Xia, X., Wang, Y., Wang, H., Wu, Y., Tao, J., Zhao, H., An, L., Li, L., Gui, K., Sun, T., Li, X., Sheng, Z., Liu, C., Yang, X., Liang, Y., Zhang, L., Kuang, X., Luo, S., and You, Y.: Five-year observation of aerosol optical properties and its radiative effects to planetary boundary layer during air pollution episodes in North China: Intercomparison of a plain site and

a mountainous site in Beijing, *Sci. Total. Environ.*, 674, 140-158, 2019.

5. Lines 98-100, I would suggest changing “due to” to “associated with”, since I do not think the economy development is the direct reason for aerosol emissions. Moreover, a few more citation could be added here, such as Yang et al. (2018, DOI: 10.1016/j.atmosres.2018.04.029), Zhao et al. (2019, doi: 10.1029/2018JD028888), Yang et al. (2019, DOI: 10.1016/j.atmosres.2019.01.027), and Li et al. (2016, doi:10.1002/2015RG000500).

Response: Thanks for the important suggestions. The words “due to” has been changed as “associated with” in the revised paper. A few more references were now added and cited as following:

Li, Z., Lau, W. K.-M., Ramanathan, V., Wu, G., Ding, Y., Manoj, M. G., Liu, J., Qian, Y., Li, J., Zhou, T., Fan, J., Rosenfeld, D., Ming, Y., Wang, Y., Huang, J., Wang, B., Xu, X., Lee, S., Cribb, M., Zhang, F., Yang, X., Takemura, T., Wang, K., Xia, X., Yin, Y., Zhang, H., Guo, J., Zhai, P., Sugimoto, N., Babu, S., Brasseur, G. P., and Zhao, C.: Aerosol and monsoon climate interactions over Asia. *Rev. Geophys.*, 54, 866–929. doi:10.1002/2015rg000500, 2016.

Yang, X., Zhao, C., Zhou, L., Li, Z., Cribb, M., and Yang, S.: Wintertime cooling and a potential connection with transported aerosols in Hong Kong during recent decades, *Atmos. Res.*, 211, 52–61, doi:10.1016/j.atmosres.2018.04.029, 2018.

Yang, Y., Zhao, C., Dong, X., Fan, G., Zhou, Y., Wang, Y., Zhao, L., Lv, F., and Yan, F.: Toward understanding the process-level impacts of aerosols on microphysical properties of shallow cumulus cloud using aircraft observations, *Atmos. Res.*, doi:10.1016/j.atmosres.2019.01.027, 2019.

Zhao, C., Wang, Y., Shi, X., Zhang, D., Wang, C., Jiang, J. H., Zhang, Q., and Fan, H.: Estimating the contribution of local primary emissions to particulate pollution using high-density station observations, *J. Geophys. Res.-Atmospheres*, doi:10.1029/2018jd028888, 2019.

6. Line 103, “pay” -> “paid”.

Response: Done. The word “pay” has been revised as “paid”.

7. Line 103-106, There are also studies about the effect of aerosol optical properties on the sea-land breeze by changing the surface radiation, such as Shen et al. (2019, doi: 10.1016/j.atmosres.2019.05.007).

Response: Thanks for the suggestions. The reference of Shen et al. (2019) about the effect of aerosol optical properties on the sea-land breeze by changing the surface radiation has been added in the revised paper.

Shen, L., Zhao, C., Ma, Z., Li, Z., Li, J., and Wang, K.: Observed decrease of summer sea-land breeze in Shanghai from 1994 to 2014 and its association with urbanization, *Atmos. Res.*, doi:10.1016/j.atmosres.2019.05.007, 2019.

8. Line 107-109, “conducted” -> “were conducted”, and some more recent studies should be cited, such as Zhang et al. (2019, doi: 10.1007/s13143-019-00125-w), and Yang et al. (2019, doi: 10.1029/2019EA000574).

Response: According to the reviewer’s suggestion, the word “conducted” has been changed as “were conducted”. Some more recent studies have been cited as follows:

Zhang, K., Zhao, C., Fan, H., Yang, Y., and Sun, Y.: Toward Understanding the Differences of PM_{2.5} Characteristics Among Five China Urban Cities, *Asia-Pac. J. Atmos. Sci.*, doi:10.1007/s13143-019-00125-w, 2019.

Yang, Y., Zhao, C., Sun, L., and Wei, J.: Improved aerosol retrievals over complex regions using NPP Visible Infrared Imaging Radiometer Suite observations, *Earth. Space. Sci.*, doi:10.1029/2019ea000574, 2019.

9. Lines 109-112, I think the aerosol optical properties should be studied over much more locations than that listed here, you may use “et al.” or other words to be more accurate. For

example, Zhao et al. (2018, doi: 10.1007/s00376-017-7069-3) have studied the aerosol properties over Xianghe, Hebei province.

Response: Thanks for the comments and suggestions. The sentences has been revised as “Many studies of aerosol optical properties were conducted in northern China with high aerosol loadings, such as the Beijing-Tianjin-Hebei region (Che et al. 2014; Xia et al., 2013; Fan et al., 2006; Xie et al., 2008; Zhang et al., 2019; Yang et al., 2019; Zhao et al., 2018). Aerosol optical properties also have been investigated at Hefei, Shouxian, Nanjing, Taihu, Shanghai and other sites in eastern China (Lee et al., 2010; He et al., 2012; Zhuang et al., 2014; Wang Z et al., 2015; Che et al., 2018).” in the revised paper to make the text more accurately.

10. Lines 126-128, I think the purpose of these aerosol properties measured are not only for evaluation of aerosol first indirect effect. We may change the description as “... can at least be used ...”.

Response: Thanks for the suggestions. The description has been revised as “The measurements of greatest interest include aerosol size distributions (volume and aerosol effective radii), optical properties (AOD, AE, SSA, absorption AOD) because those data can at least be used to evaluate direct radiative effect.”

11. Lines 135-136, “can be provided”.

Response: Done. The words have been changed as “can be provided”.

12. Line 151, delete “multi-year” since there is already “from 2010 to 2017”.

Response: Done. The words “in multi-year” have been deleted in the revises paper.

13. Line 157, there are two “five sites”, please delete one to avoid redundant.

Response: Done. The words “(five sites)” have been deleted to to avoid redundant in the revised manuscript.

14. Lines 169-171, “There are several ... that have been used at the 50 sites in this network as follows”.

Response: Thanks for the suggestions. The sentence has been modified as “There are several different types of the Cimel instruments that have been used at the 50 sites in this network as follows:” in the revised paper.

1 **Spatial distribution of aerosol microphysical and optical properties and**
2 **direct radiative effect from the China Aerosol Remote Sensing Network**

3 Huizheng Che^{1*}, Xiangao Xia^{2,3}, Hujia Zhao^{1,4}, Oleg Dubovik⁵, Brent N.
4 Holben⁶, Philippe Goloub⁵, Emilio Cuevas-Agulló⁷, Victor Estelles⁸, Yaqiang
5 Wang¹, Jun Zhu⁹ Bing Qi¹⁰, Wei Gong¹¹, Honglong Yang¹², Renjian Zhang¹³,
6 Leiku Yang¹⁴, Jing Chen¹⁵, Hong Wang¹, Yu Zheng¹, Ke Gui^{1,2}, Xiaochun
7 Zhang¹⁶, Xiaoye Zhang^{1*}

8 1 State Key Laboratory of Severe Weather (LASW) and Key Laboratory of Atmospheric
9 Chemistry (LAC), Chinese Academy of Meteorological Sciences, CMA, Beijing,
10 100081, China

11 2 Laboratory for Middle Atmosphere and Global Environment Observation (LAGEO),
12 Institute of Atmospheric Physics, Chinese Academy of Sciences, Beijing, 100029,
13 China

14 3 University of Chinese Academy of Science, Beijing, 100049, China

15 4 Institute of Atmospheric Environment, CMA, Shenyang, 110016, China

16 5 Laboratoire d'Optique Atmosphérique, Université des Sciences et Technologies de
17 Lille, 59655, Villeneuve d'Ascq, France

18 6 NASA Goddard Space Flight Center, Greenbelt, MD, USA

19 7 Centro de Investigación Atmosférica de Izaña, AEMET, 38001 Santa Cruz de
20 Tenerife, Spain

21 8 Dept. Física de la Terra i Termodinàmica, Universitat de València, C/ Dr. Moliner 50,
22 46100 Burjassot, Spain

23 9 Collaborative Innovation Center on Forecast and Evaluation of Meteorological
24 Disasters, Nanjing University of Information Science & Technology, Nanjing, 210044,
25 China

26 10 Hangzhou Meteorological Bureau, Hangzhou, 310051, China

27 11 State Key Laboratory of Information Engineering in Surveying, Mapping and Remote
28 Sensing, Wuhan University, Wuhan, 430079, China

29 12 Shenzhen Meteorological Bureau, Shenzhen, 518040, China

30 13 Key Laboratory of Regional Climate-Environment Research for Temperate East Asia,
31 Institute of Atmospheric Physics, Beijing, 100029, Chinese Academy of Sciences.

32 14 School of Surveying and Land Information Engineering, Henan Polytechnic University,
33 Jiaozuo, 454000, China

34 15 Shijiazhuang Meteorological Bureau, Shijiazhuang, 050081, China

35 16 Meteorological Observation Center, CMA, Beijing, 100081

36 Corresponding author: chehz@cma.gov.cn & xiaoye@cma.gov.cn

37 **Abstract**

38 | ~~Multi-year~~~~Long-term~~ observations of aerosol microphysical and optical
39 properties obtained through ground-based remote sensing at 50 China Aerosol
40 Remote Sensing Network (CARSNET) sites were used to characterize the
41 aerosol climatology for representative remote, rural, and urban areas over
42 China to assess effects on climate. The annual mean effective radii for total
43 particles (R_{eff}) decreased from north to south and from rural to urban sites, and
44 high total particle volumes were found at the urban sites. The aerosol optical
45 depth at 440 nm ($\text{AOD}_{440\text{nm}}$) increased from remote/rural sites (0.12) to urban
46 sites (0.79), and the extinction Ångström exponent ($\text{EAE}_{440-870\text{nm}}$) increased
47 from 0.71 at the arid/semi-arid sites to 1.15 at the urban sites, presumably due
48 to anthropogenic emissions. Single scattering albedos ($\text{SSA}_{440\text{nm}}$) ranged from
49 0.88 to 0.92 indicating slightly to strongly absorbing aerosols. Absorption
50 $\text{AOD}_{440\text{nm}}$'s were 0.01 at the remote sites versus 0.07 at the urban sites. The
51 average direct aerosol radiative effect (DARE) at the bottom of atmosphere
52 increased from the sites in the remote (-24.40 W/m^2) to the urban area
53 (-103.28 W/m^2) indicating increased cooling at the latter. The DARE for the top
54 of the atmosphere increased from -4.79 W/m^2 at the remote sites to -30.05
55 W/m^2 at the urban sites, indicating overall cooling effects for the
56 earth-atmosphere system. A classification method based on $\text{SSA}_{440\text{nm}}$, fine
57 mode fraction (FMF), and $\text{EAE}_{440-870\text{nm}}$ showed that coarse mode particles
58 (mainly dust) were dominant at the rural sites near the northwestern deserts,
59 while light-absorbing, fine-mode particles were important at most urban sites.
60 | This study will be ~~useful~~~~important~~ for understanding aerosol climate effects
61 and regional environmental pollution, and the results will provide useful
62 information for satellite validation and the improvement of climate modelings.

63 **Keywords:** aerosol optical properties; direct aerosol radiative effect; aerosol
64 type; climatology; China Aerosol Remote Sensing Network

65

66 1. Introduction

67 Atmospheric aerosols have important direct effects on climate because
68 they can scatter and absorb radiant energy and in so doing affect the Earth's
69 energy balance (Charlson et al., 1992; [Yang et al., 2016](#)). ~~Meanwhile, the~~
70 ~~aerosols can be served as cloud condensation nuclei or ice nuclei to affect the~~
71 ~~climate indirectly through aerosol–cloud interactions (Twomey et al., 1984;~~
72 ~~Garrett et al., 2006; Zhao et al., 2015; Xie et al., 2013).~~ The optical properties
73 of the aerosol determine the particles' direct effects on the Earth's radiative
74 balance and ~~weather-~~climate change (Ramanathan et al., 2001; Eck et al.,
75 2005; Myhre, 2009; [Zhao et al., 2018](#)). Aerosol optical depth (AOD) is one of
76 the key measures of the ~~total aerosol extinction~~~~aerosols'~~ effects on climate
77 (Breon et al., 2002), and the extinction Ångström exponent (EAE) ~~with spectral~~
78 ~~dependence~~ can be used ~~to obtain the information about aerosol size~~
79 ~~distribution~~~~together with AOD to study aerosol sizes and types~~ (Gobbi et al.,
80 2007; Eck et al., 1999; [Zheng et al., 2017](#)). The aerosols' absorptivity ~~depends~~
81 ~~is a key determinant of absorption on particle composition~~ ~~—is a key~~
82 ~~determinant~~ ~~—to calculate the direct aerosol~~ radiative effect (Haywood and
83 Shine, 1995; [Li et al., 2016](#); [Zheng et al., 2018](#) ~~STE~~), and the single scattering
84 albedo (SSA) is the parameter ~~has spectral dependence to distinguish major~~
85 ~~aerosol particle types~~~~needed to calculate the direct aerosol radiative effect~~
86 (Jacobson et al., 2000; Dubovik et al., 2002; Gelencser et al., 2004; Russell et
87 al., 2010; Giles et al., 2012).

88 With the recognition of the importance for climate, the aerosol optical
89 properties have been obtained from ground-based monitoring networks
90 worldwide; some of the major networks include AERONET-Aerosol Robotic
91 Network) (Holben et al., 1998) and its sub-networks of
92 PHOTONS-PHOTométrie pour le Traitement Opérationnel de Normalisation
93 Satellitaire, AEROCAN-Canadian Sun-Photometer Network, and RIMA-Iberian
94 Network for aerosol measurements ((Goloub et al., 2007; Bokoye et al., 2001;
95 Prats et al., 2011), SKYNET-SKYrad Network (Takamura and Nakajima, 2004;

96 Che et al., 2008), EARLINET-European aerosol Lidar network (Pappalardo et
97 al., 2014), the GAW-PFR Network-Global Atmosphere Watch
98 Programmer-Precision Filter Radiometers (Wehrli, 2002; Estellés et al., 2012),
99 The CARSNET-China Aerosol Remote Sensing NETwork, the
100 CSHNET-Chinese Sun Hazemeter Network and the SONET-Sun–Sky
101 Radiometer Observation Network have been established to measure aerosol
102 optical properties in China (Che et al., 2009a, 2015; Xin et al., 2007; Li et al.,
103 2018). Furthermore, the aerosol optical properties have also been used in
104 comprehensive studies of aerosol physical characteristics and chemical
105 composition [in many regions of China \(Che et al., 2009c, 2018; Zhao et al.,](#)
106 [2018\)](#).

107 China has become one of the largest aerosol sources in the world
108 [associated with](#) its rapid economic development, and this has caused
109 significant effects on local environments and regional climate (Che et al., 2005;
110 Xia, 2010; [Li et al., 2016; Yang et al., 2018, 2019; Zhao et al., 2019\)](#). There
111 have been numerous studies that have focused on aerosol optical properties
112 obtained through ground-based remote sensing methods in China (Luo et al.,
113 2002; Li et al., 2003; Duan and Mao, 2007). A few researches have ~~pay~~ [paid](#)
114 more attention to the aerosol optical properties and its radiative effects over
115 the urban-industrial areas as well as at coastal sites in northeastern [and](#)
116 [eastern](#) China (Wang et al., 2010; Xin et al., 2011; Xia et al., 2007; Zhao et al.,
117 2016; Wu et al. 2012; [Shen et al., 2019\)](#). Many studies of aerosol optical
118 properties [were](#) conducted in northern China with high aerosol loadings, such
119 as the Beijing-Tianjin-Hebei region (Che et al. 2014; Xia et al., 2013; Fan et al.,
120 2006; Xie et al., 2008; [Zhang et al., 2019; Yang et al., 2019; Zhao et al., 2018\)](#).
121 Aerosol optical properties also have been investigated at Hefei, Shouxian,
122 Nanjing, Taihu ~~and~~, Shanghai [and other sites](#) in eastern China (Lee et al., 2010;
123 He et al., 2012; Zhuang et al., 2014; Wang Z et al., 2015; Che et al., 2018).
124 Some studies of aerosol optical properties have been made in southern China
125 (Wang et al., 2015; Tao et al., 2014), and those at remote and rural sites in

126 China provide information on regional background conditions (Che et al.,
127 2009b; Wang et al., 2010; Xue et al., 2011; Zhu et al., 2014; Yuan et al., 2014).

128 China's vast size, varied terrain, and heterogeneity of aerosol sources,
129 has led to strong temporal and spatial variability in aerosol optical and physical
130 properties. The mixtures of aerosol types at most sites are complex, and
131 aerosol populations' size and composition are affected by their sources,
132 transformations that occurring during transportation and removing processes
133 (Cao et al., 2007; Wang et al., 2007; Zhang et al., 2013; Wan et al., 2015).
134 National scale, ground-based measurements of aerosol microphysical and its
135 optical properties obtained from the sunphotometer provide for a better
136 understanding of the aerosols' climate effects over the different regions of
137 China. The measurements of greatest interest include aerosol size
138 distributions (volume and aerosol effective radii), optical properties (AOD, AE,
139 SSA, absorption AOD) because those data can at least be used~~can be used~~ to
140 evaluate direct radiative effect.

141 The aim of this study was focused on the investigation of the
142 climatological spatial distribution of aerosol microphysical and optical
143 properties over regional-scales using spatial distribution data from the national
144 CARSNET network. The data were collected at CARSNET sites, which include
145 sites in the remote, rural and urban area, with the same calibration procedures
146 and calculation algorithms were used at all sites. As a result, the data are
147 directly comparable among sites (Che et al., 2009a), and the results can be
148 provided to characterize the regional distribution and temporal variation of
149 aerosol optical properties. This research focused on aerosol climate effects
150 and regional environmental pollution, and the results should be useful for
151 satellite validations and for the improvement of models in the future. The
152 remainder of this paper is organized as following: Section 2 firstly describes
153 the sites in detail, and then introduced the methods in data processing of the
154 aerosol optical properties as well as the direct aerosol radiative effect
155 calculation through the retrieved aerosol optical parameters. Section 3

156 illustrates the aerosol microphysical and optical properties, as well as its direct
157 aerosol radiative effect. An aerosol type classification method is proposed
158 according to the aerosol optical parameters. Section 4 presents the
159 conclusions of the study.

160 **2 Site description, instruments, and data**

161 **2.1 Site description**

162 Sunphotometers (CE-318, Cimel Electronique, Paris, France, see
163 Appendix A,) were installed at 50 CARSNET sites (Fig. 1) ~~in multi-year~~
164 2010 to 2017. The stations were classified as remote, rural, or urban sites
165 based on administrative division (Appendix Table 1). Three of the remote
166 stations were about more than 3000 m above the sea level on the Tibetan
167 Plateau far from the anthropogenic influences, and one of them was a
168 northwestern regional background site in China. The 23 rural sites represent (a)
169 five sites of desert regions ~~(five sites)~~ affected by most of dust aerosols
170 rather than anthropogenic particles, (b) two sites affected by both dust and
171 anthropogenic activities on the Loess Plateau, and (c) 16 sites located near or
172 surrounding the large cities relatively strong to the impacts of anthropogenic
173 activities in the central and eastern China. The last category is 24 urban sites
174 located in provincial capitals or heavily populated cities.

175 **2.2 Instruments and calibration**

176 The CE-318 sunphotometers used in this study were calibrated annually,
177 using the CARSNET calibration protocol, to verify the accuracy and reliability
178 of the sky irradiance measurements (Holben et al., 1998; Che et al., 2009; Tao
179 et al., 2014). The reference instruments for CARSNET were periodically
180 calibrated at Izaña, Tenerife, Spain located at 28.31 °N, 16.50 °W (2391.0 m
181 a.s.l.) in conjunction with the AERONET program. There ~~is~~ are several
182 different types of the Cimel instruments that have been used ~~of at~~ the 50 sites
183 in this network as follows: (1) logical type CE-318 sunphotometers (440 nm,
184 675 nm, 870 nm, 940 nm, 1020 nm and three 870 nm at the polarization band),
185 (2) numerical type CE-318 sunphotometers (440 nm, 675 nm, 870 nm, 940 nm,

186 1020 nm and three polarization bands at 870 nm), (3) numerical type CE-318
187 sunphotometers at eight wavelengths (340 nm, 380 nm, 440 nm, 500 nm, 675
188 nm, 870 nm, 940 nm, and 1020 nm), (4) and numerical type CE-318
189 sunphotometers at nine wavelengths (340 nm, 380 nm, 440 nm, 500 nm, 675
190 nm, 870 nm, 940 nm, 1020 nm and 1640 nm).

191 Measurements used to retrieve AODs were at 340 nm, 380 nm, 440 nm,
192 500 nm, 675 nm, 870 nm, 1020 nm, and 1640 nm, while the total precipitable
193 water content was obtained by using those measurements at 940 nm (Holben
194 et al., 1998; Dubovik and King, 2000). The cloud-screened AOD data were
195 calculated by using the ASTPwin software, and extinction Ångström exponents
196 (EAE) were calculated from the instantaneous AODs for wavelengths of 440
197 nm and 870 nm (Che et al., 2009, 2015). Sites with more than three daily AOD
198 observations and more than 10 monthly AOD observation days were used to
199 calculate the daily and monthly mean AODs and extinction Ångström
200 exponents. The FMF is described as the fraction of fine mode particles of total
201 AOD_{440nm} ($AOD_{fine440 nm}/AOD_{440 nm}$).

202

203 **2.3. Data processing**

204 The aerosol microphysical and optical properties, including volume size
205 distributions ($dV(r)/d\ln(r)$), the total, fine, and coarse mode aerosol effective
206 radii (R_{effT} , R_{effF} , and R_{effC} , respectively) single-scattering albedo (SSA),
207 complex refractive indices, absorption AODs (AAODs), and absorption
208 Ångström exponents (AAEs), were retrieved from the observational
209 data from the sky scattering channel of the sunphotometers at 440 nm, 670 nm,
210 870 nm, 1020 nm using the algorithms of Dubovik et al. (2002, 2006). In the
211 process of retrieval, the data of surface albedo (SA) was interpolated or
212 extrapolated to 440 nm, 670 nm, 870 nm, and 1020 nm based on the daily
213 MCD43C3 data, a product from the MODIS-Moderate Resolution Imaging
214 Spectroradiometer surface reflectance
215 (<https://ladsweb.modaps.eosdis.nasa.gov/>). The algorithm used to calculate

216 aerosol volume size distributions ($dV/\ln r$) was under the assumption of a
 217 homogeneous distribution of non-spherical particles following the approach of
 218 Dubovik (2006). The sphericity fraction retrieved from the inversions is defined
 219 as: spherical particles/(spheroidal particles + spherical particles) (Giles et al.,
 220 2011).

221 As Dubovik et al. (2002, 2006) defined that all the particles with effective
 222 radii $< 0.992 \mu\text{m}$ were considered as fine mode particles; and those > 0.992
 223 μm were considered as coarse mode particles. For the total (R_{effT}), fine (R_{effF})
 224 and coarse (R_{effC}) mode aerosols, the effective radii are calculated by the
 225 equation as follows:

$$226 \quad R_{\text{eff}} = \frac{\int_{r_{\text{min}}}^{r_{\text{max}}} r^3 \frac{dN(r)}{d\ln r} d\ln r}{\int_{r_{\text{min}}}^{r_{\text{max}}} r^2 \frac{dN(r)}{d\ln r} d\ln r} \quad (1)$$

227 Where r_{min} denotes 0.05, 0.05, 0.992 μm and r_{max} denotes 15, 0.992, 15
 228 μm of the total, fine and coarse mode particles, respectively.

229 The coarse (PV_C) and fine aerosol particle volumes distributions (PV_F) are
 230 calculated according to a bimodal lognormal function described by Whitby
 231 (1978), Shettle and Fenn (1979) and Remer and Kaufman (1998):

$$232 \quad \frac{dV(r)}{d\ln r} = \sum_{i=1}^2 \frac{C_{v,i}}{\sqrt{2\pi}\sigma_i} \exp\left[-\frac{(\ln r - \ln r_{v,i})^2}{2\sigma_i^2}\right] \quad (2)$$

233 where $C_{v,i}$ means for the volume concentration; $r_{v,i}$ means the median
 234 radius, and σ_i means the standard deviation.

235 The volume median radius is computed by fine and coarse modes
 236 particles as follows:

$$237 \quad \ln r_V = \frac{\int_{r_{\text{min}}}^{r_{\text{max}}} \ln r \frac{dV(r)}{d\ln r} d\ln r}{\int_{r_{\text{min}}}^{r_{\text{max}}} \frac{dV(r)}{d\ln r} d\ln r} \quad (3)$$

238 Then the standard deviation is calculated from the volume median radius:

带格式的: 下标

带格式的: 下标

239
$$\sigma_V = \sqrt{\frac{\int_{r_{min}}^{r_{max}} (\ln r - \ln r_V)^2 \frac{dV(r)}{d \ln r} d \ln r}{\int_{r_{min}}^{r_{max}} \frac{dV(r)}{d \ln r} d \ln r}} \quad (4)$$

240 The volume concentration ($\mu\text{m}^3/\mu\text{m}^2$) is speculated by the following
241 equation:

242
$$C_V = \int_{r_{min}}^{r_{max}} \frac{dV(r)}{d \ln r} d \ln r \quad (5)$$

243 The SSA was retrieved only for $\text{AOD}_{440\text{nm}} > 0.40$; this was done to avoid
244 the larger uncertainty inherent in the lower AOD retrieval according to Dubovik
245 et al. (2002, 2006). The AAOD and AAE for wavelength λ were calculated as
246 follows:

247
$$\text{AAOD}(\lambda) = [1 - \text{SSA}(\lambda)] \times \text{AOD}(\lambda) \quad (6)$$

248
$$\text{AAE} = \frac{-\text{dln}[\text{AAOD}(\lambda)]}{\text{dln}(\lambda)} \quad (7)$$

249 The total AODs' uncertainty was 0.01 to 0.02 according to Eck et al.
250 (1999). The accuracy of SSA retrieved from $\text{AOD}_{440\text{nm}} > 0.50$ with solar zenith
251 angles > 50 was 0.03 (Dubovik et al., 2002). The accuracy of the particle
252 volume size distribution was 15–25% between $0.1 \mu\text{m} \leq r \leq 7.0 \mu\text{m}$ and 25–100%
253 in conditions of $r < 0.1 \mu\text{m}$ and $r > 7 \mu\text{m}$.

254 Direct aerosol radiative effect (DARE in W/m^2) was calculated by the
255 radiative transfer module under cloud-free conditions, which is similar to the
256 inversion of AERONET (García et al., 2008; 2012). The DARE at the bottom of
257 the atmosphere (BOA) and the top of the atmosphere (TOA) was defined as
258 the difference in the shortwave radiative fluxes with and without aerosol effects
259 as follows:

260
261
$$\text{DARE}_{TOA} = F_{TOA}^{\uparrow 0} - F_{TOA}^{\uparrow} \quad (8)$$

262
263
$$\text{DARE}_{BOA} = F_{BOA}^{\downarrow} - F_{BOA}^{\downarrow 0} \quad (9)$$

264

265 Where F and F^0 denoted the broadband fluxes including and excluding
266 aerosols, respectively at the BOA and TOA. The “ \uparrow ” and “ \downarrow ” mean the
267 ~~upward~~downward fluxes and ~~upward~~downward fluxes, respectively.

268 In the radiative transfer module, the absorption and multiple scattering
269 effects are taken into account during flux calculations by the Discrete
270 Ordinates (DISORT) approach (Nakajima and Tanaka, 1988; Stamnes et al.,
271 1988). The gaseous distributions and single fixed aerosol vertical distribution
272 (exponential to 1 km) from the multi-layered US standard 1976 atmosphere
273 were used in the radiative flux calculations (García et al., 2008). [García et al.](#)
274 [\(2008\) pointed out that](#) the error for the observed solar radiation at the
275 surface in global was $+2.1 \pm 3.0\%$ for an overestimation of about $+9 \pm 12 \text{ Wm}^{-2}$.
276 The data used in preparing the figures for the present paper have been made
277 available as an Appendix.

278

279 **3. Results and discussion**

280 **3.1 Spatial distribution of aerosol microphysical properties**

281 A map showing the 50 CARSNET sampling sites and plots of the aerosol
282 volume size distributions ($dV/d\ln r$) at each of the sites is shown in Fig. 1.
283 Generally, the annual mean effective radius of total particles (R_{effT}) decreased
284 from the inland northwest to the southeastern coastal areas. Furthermore, the
285 volume concentration of total particles was found ~~to be~~ substantially higher at
286 the urban sites. The volume of the coarse mode particles was considerably
287 larger than that of the fine mode particles at the remotes, arid/semi-arid sites
288 and at those sites on the CLP-Chinese Loess Plateau or nearby, indicating that
289 those areas were most strongly affected by larger particles, most likely mineral
290 dust as discussed below.

291 The average (arithmetic mean) R_{effT} at the remote sites was about 0.47
292 μm with the volume about $0.05 \mu\text{m}^3/\mu\text{m}^2$ (Table 1). A large R_{effT} ($0.64 \mu\text{m}$) was
293 found at Lhasa, and the total aerosol volume there was $0.05 \mu\text{m}^3/\mu\text{m}^2$. These

294 results are consistent with those reports by Li et al. (2018) who found high
295 levels of coarse mode particles at Lhasa due to the presence of mineral dust.
296 The two other remote sites, Akedala and Shangri-La, had smaller average R_{effT}
297 values than Lhasa (0.36 and 0.39 μm , respectively), and corresponding
298 volumes were 0.06 and 0.03 $\mu\text{m}^3/\mu\text{m}^2$. The average fine-mode effective radius
299 (R_{effF}) was 0.14 μm at the remote sites, and fine-mode particle fractional
300 volume (PV_{F}) was 0.01 $\mu\text{m}^3/\mu\text{m}^2$, while the average coarse-mode effective
301 radii (R_{effC}) was 2.35 μm and the coarse-mode fractional volume (PV_{C}) was
302 0.03 $\mu\text{m}^3/\mu\text{m}^2$. These findings indicated that the contribution of coarse-mode
303 particles to the total volume of aerosol was larger at the remote sites. A study
304 by Cong et al. (2009) at the remote Nam Co site on the Tibetan Plateau
305 showed that dust particles mainly affected the site in spring, while
306 anthropogenic aerosols were prevalent in the summer.

307 The average R_{effT} at the arid and semi-arid sites (0.55 μm) was larger than
308 at the remote sites, and the total volume of aerosols at the arid/semi-arid sites
309 also was large (0.14 $\mu\text{m}^3/\mu\text{m}^2$), nearly three times that at the remote sites.
310 Large R_{effT} values (0.71 μm) were found at Tazhong, which is near the
311 | northwestern deserts, and the aerosol volume there also was high, ~~to~~ to 0.30
312 $\mu\text{m}^3/\mu\text{m}^2$. Large PV_{C} 's were found at the arid/semi-arid sites (0.05–0.27
313 $\mu\text{m}^3/\mu\text{m}^2$). The arithmetic mean R_{effT} (0.49 μm) at the rural sites on or near the
314 CLP had total aerosol volumes (0.15 $\mu\text{m}^3/\mu\text{m}^2$) similar to those at the
315 arid/semi-arid sites. These results also show a major contribution to the
316 aerosol volumes by coarse-mode particles at the sites in or near the mineral
317 dust source regions. Bi et al. (2011) similarly found that coarse particles
318 dominated the volume-size distribution at the Semi-Arid Climate and
319 Environment Observatory of Lanzhou University (SACOL) on the CLP.

320 Small R_{effT} values (0.33 μm) were found at the rural sites in eastern China,
321 and relatively high aerosol volumes were observed there (0.18 $\mu\text{m}^3/\mu\text{m}^2$). In
322 the Yangtze River Delta (YRD) region, the R_{effF} was large range for 0.16–0.17
323 μm , and the PV_{F} 's were 0.12–0.13 $\mu\text{m}^3/\mu\text{m}^2$. At the Mt. Longfeng background

324 site in northeastern China, the total particle volume was low ($0.08 \mu\text{m}^3/\mu\text{m}^2$),
325 which is consistent with minimal anthropogenic influences and low aerosol
326 loadings. Compared with the other sites, the urban areas had relatively low
327 coarse mode aerosol concentrations, but small particles were plentiful—the
328 average R_{effT} was $0.37 \mu\text{m}$ and total volume was high at $0.21 \mu\text{m}^3/\mu\text{m}^2$. The
329 average R_{effF} of fine-mode particles at the urban sites was $0.16 \mu\text{m}$ with a PV_{F}
330 of $0.10 \mu\text{m}^3/\mu\text{m}^2$ while the R_{effC} was $2.22 \mu\text{m}$ and PV_{C} was $0.11 \mu\text{m}^3/\mu\text{m}^2$.

331 The effective radii and PV_{F} values showed strong relationships with
332 population density and vehicle emissions at the urban sites. High volumes of
333 fine mode particles occurred at the northeastern urban site of Shenyang (R_{effT}
334 = $0.16 \mu\text{m}$, $PV_{\text{F}} = 0.12 \mu\text{m}^3/\mu\text{m}^2$); at major cities in northern China, including
335 Shijiazhuang ($R_{\text{effT}} = 0.16 \mu\text{m}$, $PV_{\text{F}} = 0.12 \mu\text{m}^3/\mu\text{m}^2$) and Zhengzhou ($R_{\text{effT}} =$
336 $0.18 \mu\text{m}$, $PV_{\text{F}} = 0.12 \mu\text{m}^3/\mu\text{m}^2$); at Chengdu, a city in the Sichuan Basin of
337 ($R_{\text{effT}} = 0.21 \mu\text{m}$, $PV_{\text{F}} = 0.16 \mu\text{m}^3/\mu\text{m}^2$); and at the urban regions of Nanning
338 ($R_{\text{effT}} = 0.18 \mu\text{m}$, $PV_{\text{F}} = 0.13 \mu\text{m}^3/\mu\text{m}^2$) and Panyu ($R_{\text{effT}} = 0.16 \mu\text{m}$, $PV_{\text{F}} = 0.10$
339 $\mu\text{m}^3/\mu\text{m}^2$) in southern China. Overall, these results show that the volumes of
340 fine-mode particles increased at the urban sites where anthropogenic
341 influences were most apparent.

342 Cheng et al. (2015) found different aerosol volume size distributions for
343 dust and sea salt at Shanghai in the eastern China, and they showed that their
344 relative abundances varied with season and in response to local or long-range
345 transport. Zhao et al. (2018) also reported the ~~effect~~influence of sea salt
346 aerosol on the aerosol absorption and radiative effects in the coastal region
347 ~~over of~~ northeastern China. ~~Che et al. (2018) found that aerosol hygroscopicity~~
348 ~~affected the aerosol microphysical properties in the YRD region.~~ Especially the
349 particles hygroscopic growth with different composition observed in special
350 climatic conditions could affect aerosol microphysical properties by
351 geographically variable effects (Zhang et al., 2015; Sun et al., 2010). Like in
352 the YRD region, hygroscopic growth of fine-mode particles could lead to larger
353 AOD and scattering enhancing reported by Sun et al. (2018) and Che et al.

354 (2018). Xia et al. (2019) observed the aerosol hygroscopic growth on fine
355 particle scattering coefficient in Beijing.

356 Che et al. (2018) found that aerosol hygroscopicity affected the aerosol
357 microphysical properties in the YRD region. These findings suggest that the
358 hygroscopic growth of fine-mode particles can affect aerosol microphysical
359 properties and that differences in climatic conditions could lead to
360 geographically variable effects.

带格式的：缩进：首行缩进： 0 厘米

362 3.2 Spatial distributions of AOD and EAE

363 The spatial distributions of AOD_{440 nm} and EAE_{440-870 nm} are shown in Fig. 2.
364 The AOD_{440nm} increased from the remote/rural sites to the urban sites, and as
365 one might expect, the remote sites were the least affected by particle
366 emissions and had the lowest aerosol loadings. For example, the AOD_{440nm} at
367 the remote stations was low and had an average value of 0.12. The Lhasa and
368 Shangri-La sites on the Tibetan Plateau had similar average AOD_{440nm} values
369 of 0.10. These phenomenons are similar to the study of Li et al. (2018), who
370 showed clean air conditions at Lhasa with AOD < 0.1. Cong et al. (2007, 2009)
371 also found a low AOD (0.05) at Nam Co, which was comparable to the
372 background levels at other remote sites.

373 The AOD_{440nm}'s at the arid/semi-arid sites and those on or near the Loess
374 Plateau ranged from 0.32–0.42, which is higher than at the remote sites. The
375 high AOD_{440nm} at Tazhong (0.60), which is near the deserts in northwestern
376 China was likely due to the large aerosol volume of 0.30 μm³/μm² (section 3.1)
377 caused by mineral dust. Indeed, arid and semi-arid regions in northwestern
378 China are important sources of aeolian dust on a global scale (Bi et al., 2011).
379 Li et al. (2012) showed that the contribution of dust to the average AOD at
380 SACOL near Lanzhou was 28.4%. Other sites that showed large AOD_{440nm}
381 include regions with strong anthropogenic influences, such as Dengfeng (0.79)
382 on the North China Plain, Huimin (0.83) in the YRD (0.83 to 0.87) and Huainan
383 (0.91) in the Guanzhong Plain.

384 Compared with the sites just discussed, lower AOD_{440nm} 's were found at
385 the Mt. Longfeng background station of the Northeast China Plain (0.34), the
386 semi-arid rural site as Tongyu in northeastern China (0.23), and the clean
387 Xiyong site in southern China (0.41). Zhu et al. (2014) found a low AOD of 0.28
388 at the North China Plain regional background site. Che et al. (2009c) have
389 pointed out that the large AOD at Lin'an was likely affected by the high aerosol
390 loadings in YRD Region. Among the urban sites in China, large AOD_{440nm} 's
391 were found in the cities with strong influences of anthropogenic activities, such
392 as the Northeastern Plain (Shenyang 0.89), North China Plain (Zhengzhou
393 | 0.99), Central ChinaYRD-region (Wuhan 1.00) and Sichuan Basin (Chengdu
394 1.17); the average value for these sites was 0.79. Lower AOD_{440nm} 's, that is <
395 0.50, occurred at remote sites in northwestern China, including Urumqi (0.42),
396 Yinchuan (0.37); those sites are affected less by industrial activities and the
397 population densities are lower compared with the sites in northern or eastern
398 China.

399 | It is worth noting that the particle emissions in and-or around the urban
400 sites could lead to large optical extinctions due to hygroscopic aerosol growth,
401 especially in summer when the relative humidity is often high. In a related
402 study, Zhang et al. (2018) found a large AOD of 1.10 at Wuhan in central China
403 and that was linked to secondary aerosol formation under the high
404 summertime temperatures. Li et al. (2015) similarly concluded that high
405 temperature and humidity promoted the formation of fine particles and led to
406 hygroscopic aerosol growth at Nanjing. Qin et al. (2017) observed a high
407 AOD_{500nm} of 1.04 at Shijiazhuang and related this to the hygroscopic growth of
408 aerosol fine-mode particles during polluted days.

409 Clear spatial variability in EAE values over China is evident in Fig. 3, and
410 at the remote sites, the average EAEs were 1.03. The EAE at Lhasa (0.77)
411 was lower than at Akedala (EAE = 1.13), which is in an arid region of central
412 Asia, or at Shangri-La (EAE = 1.19) in Tibet. The average coarse-mode
413 average effective radii (R_{effC}) at Lhasa was 2.26 μm and the fractional volume

414 was $0.04 \mu\text{m}^3/\mu\text{m}^2$, this result suggests the major components of the large
415 mineral dust particles in aerosol populations over that region. The smaller
416 sphericity fraction (~ 42.70) and lower FMF (0.66) at Lhasa indicates the
417 presence of non-spherical aerosol coarse particles compared with the
418 spherical fine particles in the urban sites.

419 At the arid and semi-arid sites in China, the average EAE value (0.71) was
420 relatively low and the FMF also was low (0.58). The EAE was extremely low at
421 Tazhong (0.25), which is in the Takliman Desert in the Xinjiang Uygur
422 Autonomous Region of northwestern China and the sphericity fraction (12.87)
423 and FMF (0.35) there were lower compared with most of the other sites. This
424 finding indicates a strong contribution of large particles in this desert region
425 consistent with large volume of the coarse-mode particles ($0.27 \mu\text{m}^3/\mu\text{m}^2$)
426 noted in section 3.1. The average EAE reached 0.93 at the rural sites near the
427 CLP, and the average value of FMF for those sites was 0.73. Eck et al. (2005)
428 found especially low EAE values in March and April (0.3 and 0.4, respectively)
429 at Yulin, China, where the dust aerosol dominated the optical column.

430 Large EAEs (1.23) were found at the sites in eastern China, and the FMFs
431 also were large (0.89) at those sites. This result can be attributed to the strong
432 impacts of anthropogenic in the more urbanized eastern part of the country. On
433 the other hand, large EAE values also occurred at the clean sites in
434 northeastern China, including Mt. Longfeng (1.38), where the sphericity
435 fraction was 58.5 and the FMF 0.90. This shows that small particles can have
436 stronger effects in these areas relative to some other regions of China. The
437 EAE at Lin'an was larger than that at Shangdianzi in the Northern Plain or
438 Longfengshan in Northeastern China for most months according to data from
439 Che et al. (2009c). At the urban sites, large EAEs were found at sites in
440 southern China, including Nanning (EAE = 1.36, sphericity fraction = 70.12,
441 FMF = 0.95), Panyu (EAE = 1.43, sphericity fraction = 75.55, FMF = 0.93) and
442 Zhuzilin (EAE = 1.45, sphericity fraction = 55.51, FMF = 0.94). This is likely
443 because the large populations and widespread vehicle ownership in those

444 cities led to the dominance of fine-mode particles throughout the year. Cheng
445 et al. (2015) found a uni-modal distribution of EAE centered in 1.1–1.6 with the
446 occurrence frequency about 72%, which indicated an abundance of fine
447 primary particles at Shanghai in eastern China. At the urban Nanjing site,
448 which is in east-central China, small particles were dominant, and the annual
449 average EAE was 1.21 ± 0.28 (Li et al., 2015).

450

451 **3.3 Spatial distribution of aerosol single-scattering albedo**

452 The spatial distribution of SSA at 440 nm of the 50 CARSNET stations is
453 shown in Fig. 4. As a frame of reference, Eck et al. (2005) reported that that
454 SSA_{440nm} from the AERONET retrievals were 0.82 to 0.98 globally. We note
455 that SSA_{440nm} values in this range reflect slightly to strongly absorbing aerosols,
456 and these particles originate from ~~a~~ multitude ~~of~~ sources (Che et al., 2018).
457 The SSA_{440nm} 's decreased from remote/rural to the urban sites and from west
458 to east, which means that there were higher percentages of absorbing
459 particles at the urban and eastern stations. The average SSA_{440nm} at the
460 remote sites was about 0.91, which is indicative of particles with moderate
461 absorption. The absorbing aerosols at the remote sites were more ~~than~~-likely
462 mineral dust particles because those sites are less likely to be affected by
463 carbonaceous particles, which also are absorbing, but mainly produced by
464 anthropogenic activities. The SSA_{440nm} 's for the arid and semi-arid sites were
465 0.89. The relatively high SSA at Tazhong (0.92) was probably due to slightly
466 absorbing, coarse mode dust particles (~~EAE-EAE =~~ 0.25).

467 A study by Bi et al. (2011) showed that SSAs increased slightly with
468 wavelength when dust was present at the SACOL site. Moderately absorbing
469 particles were found in our study on or near the Chinese Loess Plateau where
470 the SSA_{440nm} 's were typically 0.88 to 0.89. Eck et al. (2005) concluded that the
471 spectral SSA demonstrated effects of dust at Yulin because the SSA increased
472 for wavelengths from 440 to 675 nm. At the rural sites in eastern China, large
473 SSA_{440nm} 's mainly occurred at sites in the YRD affected anthropogenic

474 influences; these include Tonglu (0.93), Xiaoshan (0.93), Xiyong (0.94). Che et
475 al. (2018) found the slightly absorbing particles came from industrial activity
476 and anthropogenic sources at YRD region with the $SSA_{440\text{ nm}}$ between 0.91 to
477 0.94.

478 The average value of $SSA_{440\text{ nm}}$ at the urban sites was 0.90, which
479 indicates that particles with moderate absorption dominated the aerosol
480 populations. Cheng et al. (2015) reported a seasonal range of SSA from 0.88
481 to 0.91 at Shanghai, with higher values in autumn and winter compared with
482 spring and summer. Lower $SSA_{440\text{ nm}}$'s occurred at the urban sites and
483 industrial regions in northeastern China, such as Shenyang (0.84), Anshan
484 (0.89), Fuhsun (0.84), which indicates that the particles were more strongly
485 absorbing in that region. On the other hand, higher $SSA_{440\text{ nm}}$'s were found at
486 urban sites in southern China, including Nanning (0.92), Panyu (0.90) and
487 Zhuzilin (0.96), and this indicates that the particles at those sites were slightly
488 or weakly absorbing.

489 Moreover, we found that the $SSA_{440\text{ nm}}$ spatial distribution reflected the
490 percentages of absorbing aerosols at the urban sites both in northern and
491 eastern China. The reports of Dubovik et al. (2000, 2002, 2006) showed that
492 SSA values vary with both particle size and composition, and Su et al. (2017)
493 used the variations in SSA with wavelength to indicate the presence of brown
494 carbon aerosols at Tianjin, a coastal megacity in China. Qin et al. (2017)
495 suggested that the small SSAs found at Shijiazhuang indicated the presence
496 of fine-mode absorbing particles, such as brown carbon. Zhuang et al. (2014)
497 reported that the SSA at the Nanjing urban site ranged from 0.90 to 0.95, and
498 the aerosol was more absorbing in fall/autumn, possibly due to the biomass
499 burning emission in the YRD. As evident in the results presented in section 3.1,
500 one can see that the R_{effT} , R_{effF} and R_{effC} between northeastern and southern
501 China was very similar. For example, at Shenyang, a megacity in northeastern
502 China, the effective radii of total, fine- and coarse-mode particles were 0.31,
503 0.16, 2.23 μm and the corresponding volumes were 0.22, 0.12, 0.10 $\mu\text{m}^3/\mu\text{m}^2$,

504 respectively. At Hangzhou in the YRD region, the R_{effT} , R_{effF} and R_{effC} were 0.30,
505 0.17, 2.21 μm with the volumes about 0.22, 0.12, 0.10 $\mu\text{m}^3/\mu\text{m}^2$, respectively.
506 Therefore, the different $\text{SSA}_{440\text{nm}}$ distributions in the two regions may be
507 attributed by the special aerosol composition related to the urban-industrial
508 background of northeastern China (lower $\text{SSA}_{440\text{nm}}$) and more
509 anthropogenic sources in the eastern China environmental (higher
510 $\text{SSA}_{440\text{nm}}$).

511 Dust aerosols with light-absorbing occur more frequently in spring in
512 northeastern China than in more southern regions (Zhao et al., 2018).
513 Anthropogenic emissions from seasonal biomass burning and residential
514 heating are two other main factors that affect aerosol composition between the
515 two regions (Che et al., 2018). Especially in winter, there was high percentage
516 of absorbing aerosols at the northeastern sites, and that was more than likely
517 caused by emissions of carbonaceous aerosol from residential heating (Zhao
518 et al., 2015). Climatic conditions are also the main factors affecting the
519 absorption characteristics of aerosols in different regions of north and south
520 China. The increased light scattering could well be due to the particles
521 hygroscopic growth demonstrated in other studies. For example, Mai et al.
522 (2018) found that AODs and SSAs both increased with relative humidity at
523 Guangdong in the PRD region, which suggests that condensational growth
524 can affect the aerosol optical properties.

525

526 **3.4 Spatial distributions of absorption aerosol optical depth (AAOD)**

527 The spatial distribution of AAOD at 440 nm shown as Fig. 5 indicates that
528 overall, the $\text{AAOD}_{440\text{nm}}$'s increased from north to south and from remote/rural
529 to urban sites. Lower $\text{AAOD}_{440\text{nm}}$'s were found at the remote stations, where
530 the average value was 0.01. The $\text{AAOD}_{440\text{nm}}$ at Akedala, a remote site in
531 northwestern China, was 0.02, and that was higher than at Shangri-La or
532 Lhasa (0.01), both of which are on the Tibetan Plateau. The low $\text{AAOD}_{440\text{nm}}$'s
533 throughout that region indicates that the aerosol population was not strongly

534 absorbing. Compared with these three sites, the average $AAOD_{440nm}$'s at the
535 arid and semi-arid sites were higher (0.03); for example, an $AAOD_{440nm}$ of
536 0.05 was found at Tazhong, which is adjacent to the desert, and that indicates
537 that the aerosol particles were more absorbing. As discussed in sections 3.2
538 and 3.3, dust aerosols likely make a significant contribution to aerosol light
539 absorption in the areas impacted by the deserts.

540 The low $AAOD_{440nm}$ found at Xilinhot (0.02) was probably due to the low
541 aerosol loadings ($AOD_{440nm} = 0.21$) in this region. The $AAOD_{440nm}$'s at the Mt.
542 Gaolan and Yulin rural sites which on or around the CLP were about 0.04 and
543 0.03, respectively, and the particles were moderately absorbing ($SSA = 0.89$).
544 The large $AAOD_{440nm}$ at Datong (0.09) can be explained by the high AOD_{440nm}
545 (0.58) there. Indeed, large $AAOD_{440nm}$'s were found at rural sites in eastern
546 China, where there were high AODs and low SSAs as noted in sections 3.2
547 and 3.3. Of these sites, Dengfeng ($AOD_{440nm} = 0.08$) and Huimin ($AOD_{440nm} =$
548 0.08) are located on the North China Plain, while Huainan ($AOD_{440nm} = 0.10$) is
549 on the Guanzhong Plain. Lower $AAOD_{440nm}$'s, from 0.02–0.03, occurred at
550 Tongyu (0.03), which is at a semi-arid region in northeastern China, at the Mt.
551 Longfeng (0.03) regional background site on the Northeast China Plain, at the
552 Yushe rural site in northern China (0.03), and at the clean Xiyong site in the
553 PRD (0.02).

554 Several urban sites showed $AAOD_{440nm}$ values greater than 0.10; these
555 include Fushun (0.11) and Shenyang (0.14) in the northeastern China,
556 Lanzhou (0.10) in the northwestern China, and Nanjing (0.10) and Wuhan
557 (0.11) in the eastern and central China. Lower $AAOD_{440nm}$'s occurred in other
558 urban areas, such as Yinchuan ($AAOD_{440nm} = 0.02$, $AOD_{440nm} = 0.37$) in the
559 northwest and Zhuzilin ($AAOD_{440nm} = 0.03$, $AOD_{440nm} = 0.66$) in the PRD; both
560 of these sites had relatively low AOD_{440} 's indicating weaker anthropogenic
561 influences compared with metropolitan regions of some other areas. We note
562 that there are significant uncertainties in relating aerosol absorbing properties
563 to particle types, such as black carbon, organic matter, as well as mineral dust

564 (Russell et al., 2010; Giles et al., 2012). Nonetheless, the information
565 presented here on the spatial distribution of AODs over China may be useful
566 for the further investigations into the relationships between light absorption and
567 particle type (Liu et al., 2017; Schuster et al., 2016a, 2016b).

568

569 | **3.5 Spatial distribution of direct aerosol ~~direct~~-radiative effect at the** 570 **Earth's surface and top of the atmosphere**

571 The spatial distributions of the DAREs calculated for both the bottom and
572 top of the atmosphere are shown in Fig. 6. Overall, the DARE-BOAs increased
573 from northwest to southeast and from rural to urban sites, consistent with
574 impacts from the densely populated regions around the sites. The average
575 DARE-BOA at the remote sites was -24.40 W/m^2 , and in comparison, a higher
576 DARE-BOA (-33.65 W/m^2) occurred at Akedala, which occurred on a remote
577 region of northwestern China. The $\text{AOD}_{440\text{nm}}$ at Akedala was relatively low
578 (0.17) and the SSA moderate (0.90). The moderate absorption of aerosol could
579 lead to more strong surface cooling effects with little higher DARE-BOA than
580 the other remote sites. The DARE-BOAs for Lhasa and Shangri-La were
581 | -22.13 and -17.43 W/m^2 , respectively. These results indicate weaker surface
582 cooling effects at the remote sites relative to other regions because the aerosol
583 loadings were relatively low, as indicated by $\text{AOD}_{440\text{nm}}'s < 0.20$.

584 The average DARE-BOTs at the arid and semi-arid sites of China were
585 about -56.43 W/m^2 , and those high DARE-BOAs can be explained by the
586 moderately absorbing particles ($\text{SSA} = 0.89$) and large $\text{AOD}_{440\text{nm}}'s$ (0.32)
587 compared with the remote sites. A large DARE-BOA (-91.20 W/m^2) occurred at
588 the Tazhong site near the northwestern deserts, and there, the high AOD (0.60)
589 and the slight absorption of mineral dust ($\text{SSA} = 0.92$) imply substantial surface
590 cooling. The average DARE-BOA for rural sites on the Chinese Loess Plateau
591 or surrounding was -74.67 W/m^2 , and that also implies cooling at the surface.

592 Several rural sites in northern and eastern China had large DARE-BOA
593 values; these include Huimin (-111.58 W/m^2), Dengfeng (-104.78 W/m^2) and

594 Huainan (-129.17 W/m^2), and at those sites the AODs were high, from 0.80–
595 0.90, and the SSAs were ~ 0.89 . These results show stronger surface cooling
596 effects at sites influenced by anthropogenic emissions compared with the
597 remote sites or those near the deserts. The large negative DARE-BOA values
598 (-103.28 W/m^2) at the urban sites indicate that the combination of high
599 $\text{AOD}_{440\text{nm}}$'s (0.79) and moderate SSAs (0.90) can cause significant surface
600 cooling. Indeed, anthropogenic emissions presumably led to the high
601 DARE-BOAs at urban sites, including Shenyang (-144.88 W/m^2) and Fushun
602 (-116.91 W/m^2) in the Northeastern Plain, Xian in the Guanzhong Plain
603 (-132.55 W/m^2), Chengdu in the Sichuan Basin (-110.42 W/m^2), Lanzhou in the
604 western region (-126.17 W/m^2), and Nanjing (-143.38 W/m^2) and Wuhan
605 (-171.80 W/m^2) in the Central China ~~YRD~~. These results indicate that
606 anthropogenic aerosols can cause significant direct radiative effects at urban
607 sites.

608 The DARE-TOAs increased from north to south and from rural to urban
609 sites, and the average DARE-TOA for the remote stations was low, about -4.79
610 W/m^2 (Fig. 7). The DARE-TOAs at Lhasa and Shangri-La were -5.04 W/m^2
611 and -8.93 W/m^2 , respectively. A notably small DARE-TOA was found at
612 Akedala (-0.42 W/m^2), indicating that the effects of the aerosol on the
613 temperature of earth-atmosphere system there would be weak. The average
614 DARE-TOA at the arid and semi-arid sites was -10.17 W/m^2 . The large
615 DARE-TOA found at Tazhong (-23.49 W/m^2) could represent the larger
616 contribution of slightly absorbing mineral aerosols ($\text{SSA} \approx 0.92$) and a large
617 AOD (0.60); this indicates more cooling at surface through the absorption and
618 scattering solar radiation compared with the less impacted sites. This is
619 consistent with the results for Tazhong discussed in section 3.1 which showed
620 high volumes of coarse mode particles with large radii.

621 The average DARE-TOA at rural sites on the Chinese Loess Plateau or
622 nearby was about -14.56 W/m^2 . Although the $\text{SSA}_{440\text{nm}}$ were close to Gaolan
623 and Yulin about 0.89, the TOAs were quite different (Mt. Gaolan -20.87 W/m^2 ;

624 Yulin -9.09 W/m^2) which could be due to the different $\text{AOD}_{440\text{nm}}$ about 0.36 and
625 0.32, respectively. In rural eastern China, the DARE-TOA was about -32.40
626 W/m^2 , and to put this in context, Che et al. (2018) found that DARE-TOAs of
627 -40 W/m^2 at rural sites in the YRD region, which is indicative of a relatively
628 strong cooling effect. Low DARE-TOAs were found at the Mt. Longfeng rural
629 site in northeastern China (DARE-TOA = -11.34 , $\text{AOD}_{440\text{nm}} = 0.34$, $\text{SSA} = 0.89$)
630 and at the Tongyu semi-arid site in northeastern China as (DARE-TOA = -8.87 ,
631 $\text{AOD}_{440\text{nm}} = 0.23$, $\text{SSA} = 0.88$) where the aerosol loadings were relatively low
632 and the absorption was moderate.

633 In the urban sites at central and eastern China, the average DARE-TOA
634 values were about -30.05 W/m^2 . Higher DARE-TOAs occurred at Anshan in
635 the Northeastern Plain (-39.66 W/m^2), Chengdu in the Sichuan Basin ~~as~~
636 (-52.21 W/m^2), Hangzhou in the YRD (-40.16 W/m^2), Jiaozuo (-39.35 W/m^2)
637 and Zhengzhou (-46.18 W/m^2) in the North China Plain, and Zhuzilin (-40.15
638 W/m^2) in the PRD region. The high DARE-TOA values at these urban sites
639 imply relatively strong cooling effects due to higher aerosol loadings in the
640 atmosphere moderate to strong light absorption by the particles.

641

642 **3.6 Spatial distributions of aerosol mixing properties**

643 The spatial distribution of aerosol mixing properties (Figure 8) was
644 obtained by using the $\text{SSA}_{440\text{nm}}$, FMF, and EAE results to classify the particles
645 based on size and absorbing properties. In previous studies by Zheng et al.
646 (2017) and Che et al. (2018), the particles in this study were grouped into eight
647 types as Table 2 show. Moreover, the FMF has been provided to give the
648 particle size information in the group of the particles.

649 At the remote Akedala and Lhasa sites (FMF = 0.70 – 0.78 and $\text{SSA}_{440\text{nm}} =$
650 0.85), the percentages of mixed absorbing particles (Type V) were 35–40%,
651 while at Shangri-la (FMF = 0.76 , $\text{SSA}_{440\text{nm}} = 0.84$), the percentage was slightly
652 lower, 24.62%. The characteristics of the particles at these remote,
653 high-altitude sites were probably affected by the rugged topography which

654 would promote particle mixing. The proportion of coarse mode, mainly dust,
655 particles with moderate to strong absorption (Group VII) was highest at the arid
656 and semi-arid sites. The percent abundances of Group VII particles were 57.90%
657 at Dunhuang ($AE = 0.26$, $SSA_{440nm} = 0.85$, $FMF = 0.43$) and 58.52% at
658 Tazhong ($AE = 0.20$, $SSA_{440nm} = 0.87$, $FMF = 0.37$), respectively. Mixed
659 absorbing particles (Type V) and strongly absorbing dust particles (Group VII)
660 accounted for 30 to 70% of the aerosol in the rural sites on or near the CLP.
661 The percentages of mixed absorbing particles (Type V) at Gaolan, Yulin, and
662 Datong were 31.98%, 45.22% and 29.04%, respectively, and the average
663 FMFs at those sites ranged from 0.70–0.76.

664 The proportions of the coarse-mode aerosols with strongly absorbing in
665 Group VII were about 35.23% at Gaolan and 21.21% at Yulin, which was
666 mainly dust particles with the FMFs at those sites were 0.43 and 0.48,
667 respectively. The proportion of coarse-mode particles with strongly absorbing
668 in Group VII and coarse-mode particles with weakly-absorbing in Group VIII at
669 the rural sites in eastern China were < 11%. These patterns indicated that the
670 differences in the eastern region from northwestern China because in the east,
671 coarse-mode particles have only a minor contribution to aerosol absorption.
672 The percentage of fine-mode particles with weakly-absorbing in Type IV and
673 mixed absorbing particles in Type V combined about ~50% at the eastern sites.
674 This result suggests that mixed aerosols originated from a variety of sources
675 and that many of the sites were affected by anthropogenic emissions from
676 megacities upwind.

677 The fine-mode particles with absorbing in Types I, II, III and V accounted
678 for 50 to 90% at most of the urban sites. The percentages of these four particle
679 types combined were especially large in eastern China; for example, at Panyu,
680 particle Types I–IV composed 90.83% of the total, and the FMF there was
681 0.90–0.94, while at Zhuzilin, the percentage of Types I–IV was 92.55%, and
682 the FMF was 0.92–0.94. These results are another indication that fine-mode
683 particles are important for light absorption in urban areas. In contrast, the

684 Lanzhou and Urumqi urban sites were less affected by absorbing fine-particles
685 because the percentages of Type I–IV particles were only 19.73% and 18.36%,
686 respectively. The mixed absorbing Type V particles accounted for large
687 percentages of the total at Lanzhou (48.80%, EAE = 0.88, SSA = 0.82, FMF =
688 0.73) and at Urumqi (59.39%, EAE = 0.94, SSA = 0.84, FMF = 0.75). Different
689 from the other urban sites, these patterns show that larger particles had
690 significant contributions to the aerosol absorption at these two northwestern
691 sites.

692

693 **4. Conclusions**

694 Aerosol microphysical and its optical properties obtained from the
695 ground-based sunphotometer deployed at 50 CARSNET stations were used to
696 begin the development of their climatology characteristics and to investigate
697 potential aerosol-climate effects over vast area of China. Direct aerosol
698 radiative effects (DAREs) at the bottom and at the top of the atmosphere were
699 calculated, and eight types of aerosols were classified based on the particle
700 size and absorbing properties. The annual mean values of the ReffT
701 decreased from the arid and semi-arid sites ($0.55 \mu\text{m}$) to the urban sites (0.37
702 μm). The aerosol volumes increased from the remote sites ($0.05 \mu\text{m}^3/\mu\text{m}^2$) to
703 the urban sites ($0.21 \mu\text{m}^3/\mu\text{m}^2$). The volumes of coarse-mode particle were
704 larger than those for the fine mode at the remote and arid/semi-arid sites—this
705 can be explained by the greater relative abundances of mineral dust compared
706 with pollution-derived particles at those sites. At the urban sites, where
707 anthropogenic influences were relatively strong, the proportion of fine mode
708 particles increased gradually with aerosol volume.

709 The $\text{AOD}_{440\text{nm}}$ progressively increased from the remote sites (0.12) to the
710 arid and semi-arid sites (0.32) to rural sites in eastern China (0.70) and finally
711 to the urban sites (0.79), which were the ones most strongly affected by
712 anthropogenic activities. The average $\text{EAE}_{440-870 \text{ nm}}$'s at the arid and semi-arid
713 sites were relatively low (0.71), which indicates an important contribution of

714 larger particles to the aerosol extinction in those regions. The consistently
715 large $EAE_{440-870\text{ nm}}$'s at the urban sites (> 1.20) and the high FMFs that those
716 site (0.88) are the evidence that fine mode particles are prevalent throughout
717 year. The average $SSA_{440\text{ nm}}$'s at the remote, rural, and urban sites were
718 relatively similar, averaging about 0.89, and this indicates the particles were
719 moderately absorbing.

720 Overall, dust aerosols with light-absorbing in spring and emissions came
721 from biomass burning and residential heating during the colder months were
722 the main factors that led to spatial differences in the percentages of absorbing
723 aerosols over China. The $AAOD_{440\text{ nm}}$'s increased from the remote sites (0.01)
724 to the arid and semi-arid sites (0.03) to the rural sites of eastern China (0.05)
725 and finally to the urban sites (0.07). High $AAOD_{440\text{ nm}}$'s were caused by
726 light-absorbing dust aerosols at the rural sites and by the strong anthropogenic
727 emissions in the metropolitan areas. The spatial patterns in the absorbing
728 aerosols were not only affected by the chemical composition of aerosol, but
729 also by physical effects imposed by topography, weather, and climate.

730 The average DARE-BOA values were -24.40 W/m^2 at the remote sites;
731 -56.43 W/m^2 at the arid and semi-arid sites; -74.67 W/m^2 at the sites on the
732 CLP or nearby; -85.25 W/m^2 at the rural sites in eastern China; and -103.28
733 W/m^2 at the urban sites. The larger DARE-BOA values at the urban sites imply
734 stronger cooling effects from anthropogenic emissions compared with those
735 from mineral dust at the remote sites or those near the desert. Moreover, larger
736 DARE-TOA's also occurred at the urban sites (-30.05 W/m^2), which indicates
737 strong cooling effects due to the large aerosol extinctions between the
738 earth-atmosphere system displayed the moderate to strong light absorption.
739 Mixed-absorbing particles were the most abundant aerosol type in the remote
740 and rural sites on or near the Chinese Loess Plateau and in eastern China.
741 Mineral dust particles with moderate to strong absorbing were dominant in the
742 arid and semi-arid sites while absorbing fine-mode particles accounted for 50
743 to 90% of the aerosol at the most urban sites.

744 The results of the study have considerable value for ground truthing
745 satellite observations and for validating aerosol models. Moreover, the results
746 also have provided significant information on aerosol optical and radiative
747 properties for different types of sites covering a broad expanse of China.
748 These results also are a major step towards developing a climatology for
749 aerosol microphysical and optical properties for China and even East Asia.

750 **Data availability:**

751 The detailed CARSNET AOD dataset used in the study can be requested
752 by contacting the corresponding author.

753 **Competing interests.**

754 The authors declare that they have no conflict of interest.

755 **Author contribution:**

756 All authors contributed to shaping up the ideas and reviewing the paper.
757 HC, XX and XZ designed and implemented the research, as well as prepared
758 the manuscript; HC, HZ, YW and HW contributed to analysis of the CARSNET
759 dataset; HC, XX, JZ, OD, BNH, PG, and ECA contributed to the CARSNET
760 data retrieval; HC, BQ, WG, HY, RZ, LY, JC, YZ, KG, and XZ carried out the
761 CARSNET observations; OD, BNH, PG, and ECA provided constructive
762 comments on this research.

763 **Acknowledgments**

764 This work was supported by grants from the National Science Fund for
765 Distinguished Young Scholars (41825011), the National Key R & D Program
766 Pilot Projects of China (2016YFA0601901), National Natural Science
767 Foundation of China (41590874), the CAMS Basis Research Project
768 (2017Z011), the European Union Seventh Framework Programme
769 (FP7/2007-2013) under grant agreement no. 262254. AERONET-Europe
770 ACTRIS-2 program, European Union's Horizon 2020 research and innovation
771 programme under grant agreement No 654109.

772

773 **References**

774 Bi, J.R., Huang, J.P., Fu, Q., Wang, X., Shi, J.S., Zhang, W., Huang, Z.W., and
775 Zhang, B.D.: Toward characterization of the aerosol optical properties
776 over Loess Plateau of Northwestern China, *Journal of Quantitative*
777 *Spectroscopy and Radiative Transfer*, 112, 346-360,
778 <https://doi.org/10.1016/j.jqsrt.2010.09.006>, 2011.

779 Bokoye, A.I., Royer, A., O'Neill, N.T., Cliche, P., Fedosejevs, G., Teillet, P.M.,
780 and McArthur, L.J.B.: Characterization of atmospheric aerosols across
781 Canada from a Ground-based sun photometer network: Aerocan, *Atmos.*
782 *Ocean.*, 39, 429–456, <https://doi.org/10.1080/07055900.2001.9649687>,
783 2001.

784 Breon, F., Tanré, D., and Generoso, S.: Aerosols effect on the cloud droplet
785 size monitored from satellite, *Science*, 295, 834-838,
786 <https://doi.org/10.1126/science.1066434>, 2002.

787 Cao, J.J., Lee, S.C., Chow, J.C., Watson, J.G., Ho, K.F., Zhang, R.J., Jin, Z.D.,
788 Shen, Z.X., Chen, G.C., Kang, Y.M., Zou, S.C., Zhang, L.Z., Qi, S.H., Dai,
789 M.H, Cheng, Y., and Hu, K.: Spatial and seasonal distributions of
790 carbonaceous aerosols over China, *J. Geophys. Res.*, 112, D22S11.
791 <http://dx.doi.org/10.1029/2006JD008205>, 2007.

792 Charlson, R. J., Schwartz, S. E., Hales, J. M., Cess, D., Coakley, J. A., and
793 Hansen, J. E.: Climate forcing by anthropogenic aerosols, *Science*, 255,
794 423–430, <https://doi.org/10.1126/science.255.5043.423>, 1992.

795 Che, H.Z., Shi, G.Y., Zhang, X.Y., Arimoto, R., Zhao, J.Q., Xu, L., Wang, B.,
796 and Chen, Z.H.: Analysis of 40 years of solar radiation data from China,
797 1961-2000, *Geophysical Research Letters*, 32, L06803,
798 <https://doi.org/10.1029/2004GL022322>, 2005.

799 Che, H., Shi, G., Uchiyama, A., Yamazaki, A., Chen, H., Goloub, P., and Zhang,
800 X.: Intercomparison between aerosol optical properties by a PREDE
801 skyradiometer and CIMEL sunphotometer over Beijing, China, *Atmos.*
802 *Chem. Phys.*, 8, 3199–3214, <http://dx.doi.org/10.5194/acp-8-3199-2008>,
803 2008.

804 Che, H., Zhang, X., Chen, H., Damiri, B., Goloub, P., Li, Z., Zhang, X., Wei, Y.,
805 Zhou, H., Dong, F., Li, D., and Zhou, T.: Instrument calibration and aerosol
806 optical depth (AOD) validation of the China Aerosol Remote Sensing
807 Network (CARSNET), *J. Geophys. Res.*, 114, D03206,
808 <https://doi.org/10.1029/2008JD011030>, 2009a.

809 Che, H. Z., Zhang, X. Y., Alfraro, S., Chatenet, B., Gomes, L., and Zhao, J. Q.:
810 Aerosol optical properties and its radiative forcing over Yulin, China in
811 2001 and 2002, *Adv. Atmos. Sci.*, 26, 564–576,
812 <https://doi.org/10.1007/s00376-009-0564-4>, 2009b.

813 Che, H. Z., Yang, Z. F., Zhang, X. Y., Zhu, C. Z., Ma, Q. L., Zhou, H. G., and
814 Wang, P.: Study on the aerosol optical properties and their relationship
815 with aerosol chemical compositions over three regional background
816 stations in China, *Atmospheric Environment*, 43, 1093–1099,
817 <https://doi.org/10.1016/j.atmosenv.2008.11.010>, 2009c.

818 Che, H., Xia, X., Zhu, J., Li, Z., Dubovik, O., Holben, B., Goloub, P., Chen, H.,
819 Estelles, V., Cuevas-Agulló, E., Blarel, L., Wang, H., Zhao, H., Zhang, X.,
820 Wang, Y., Sun, J., Tao, R., Zhang, X., and Shi, G.: Column aerosol optical
821 properties and aerosol radiative forcing during a serious haze-fog month
822 over North China Plain in 2013 based on ground-based sunphotometer
823 measurements, *Atmos. Chem. Phys.*, 14, 2125–2138,
824 <https://doi.org/10.5194/acp-14-2125-2014>.

825 Che, H., Zhang, X.-Y., Xia, X., Goloub, P., Holben, B., Zhao, H., Wang, Y.,
826 Zhang, X.-C., Wang, H., Blarel, L., Damiri, B., Zhang, R., Deng, X., Ma, Y.,
827 Wang, T., Geng, F., Qi, B., Zhu, J., Yu, J., Chen, Q., and Shi, G.:
828 Ground-based aerosol climatology of China: aerosol optical depths from
829 the China Aerosol Remote Sensing Network (CARSNET) 2002–2013,
830 *Atmos. Chem. Phys.*, 15, 7619–7652, [https://doi.org/10.5194/acp-](https://doi.org/10.5194/acp-15-7619-2015)
831 [15-7619-2015](https://doi.org/10.5194/acp-15-7619-2015), 2015.

832 Che, H., Qi, B., Zhao, H., Xia, X., Eck, T.F., Goloub, P., Dubovik, O., Estelles,
833 V., Cuevas-Agulló, E., Blarel, L., Wu, Y., Zhu, J., Du, R., Wang, Y., Wang,

834 H., Gui, K., Yu, J., Zheng, Y., Sun, T., Chen, Q., Shi, G., and Zhang X.:
835 Aerosol optical properties and direct radiative forcing based on
836 measurements from the China Aerosol Remote Sensing Network
837 (CARSNET) in eastern China, *Atmospheric Chemistry and Physics*, 18,
838 405–425, <https://doi.org/10.5194/acp-18-405-2018>, 2018.

839 Cong, Z.Y., Kang, S.C., Liu, X.D., and Wang, G.F.: Elemental composition of
840 aerosol in the Nam Co region, Tibetan Plateau, during summer monsoon
841 season, *Atmospheric Environment*, 41, 1180–1187,
842 <https://doi.org/10.1016/j.atmosenv.2006.09.046>, 2007.

843 Cong, Z.Y., Kang, S.C., Smirnov, A., and Holben, B.: Aerosol optical properties
844 at Nam Co, a remote site in central Tibetan Plateau, *Atmospheric
845 Research*, 92, 42–48, <https://doi.org/10.1016/j.atmosres.2008.08.005>,
846 2009.

847 Duan, J. and Mao, J.: Study on the distribution and variation trends of
848 atmospheric aerosol optical depth over the Yangtze River Delta, *Acta
849 Scien. Circum.*, 27, 537–543,
850 https://doi.org/10.1007/978-1-4020-6475-3_126, 2007.

851 Dubovik, O. and King, M. D.: A flexible inversion algorithm for retrieval of
852 aerosol optical properties from sun and sky radiance measurements, *J.
853 Geophys. Res.*, 105, 20673–20696,
854 <https://doi.org/10.1029/2000JD900282>, 2000.

855 Dubovik, O., Holben, B. N., Eck, T. F., Smirnov, A., Kaufman, Y. J., King, M. D.,
856 Tanre, D., and Slutsker, I.: Variability of absorption and optical properties
857 of key aerosol types observed in worldwide locations, *J. Atmos. Sci.*, 59,
858 590–608,
859 [https://doi.org/10.1175/1520-0469\(2002\)059<0590:VOAAOP>2.0.CO;2](https://doi.org/10.1175/1520-0469(2002)059<0590:VOAAOP>2.0.CO;2),
860 2002.

861 Dubovik, O., Sinyuk, A., Lapyonok, T., Holben, B. N., Mishchenko, M., Yang, P.,
862 Eck, T. F., Volten, H., Munoz, O., Veihelmann, B., van der Zande, W. J.,
863 Leon, J. F., Sorokin, M., and Slutsker, I.: Application of spheroid models to

864 account for aerosol particle nonsphericity in remote sensing of desert dust,
865 J. Geophys. Res.-Atmos., 111, D11208,
866 <https://doi.org/10.1029/2005JD006619>, 2006.

867 Dubuisson, P., Buriez, J. C., and Fouquart, Y.: High spectral resolution solar
868 radiative transfer in absorbing and scattering media, application to the
869 satellite simulation, J. Quant. Spectrosc. Ra., 55, 103–126,
870 [https://doi.org/10.1016/0022-4073\(95\)00134-4](https://doi.org/10.1016/0022-4073(95)00134-4), 1996.

871 Eck, T. F., Holben, B. N., Reid, J. S., Dubovik, O., Smirnov, A., O'Neill, N. T.,
872 Slutsker, I., and Kinne, S.: Wavelength dependence of the optical depth of
873 biomass burning, urban, and desert dust aerosols, J. Geophys. Res., 104,
874 31333–31349, <https://doi.org/10.1029/1999jd900923>, 1999.

875 Eck, T. F., Holben, B. N., Dubovik, O., Smirnov, A., Goloub, P., Chen, H. B.,
876 Chatenet, B., Gomes, L., Zhang, X. Y., Tsay, S. C., Ji, Q., Giles, D., and
877 Slutsker, I.: Columnar aerosol optical properties at AERONET sites in
878 central eastern Asia and aerosol transport to the tropical Mid-Pacific, J.
879 Geophys. Res., 110, D06202, <https://doi.org/10.1029/2004JD005274>,
880 2005.

881 Estellés, V., Campanelli, M., Utrillas, M. P., Expósito, F., and Martínez-Lozano,
882 J. A.: Comparison of AERONET and SKYRAD4.2 inversion products
883 retrieved from a Cimel CE318 sunphotometer, Atmos. Meas. Tech., 5,
884 569–579, <https://doi.org/10.5194/amt-5-569-2012>, 2012.

885 Fan, X., Chen, H., Goloub, P., Xia, X., Zhang, W., and Chatenet, B.: Analysis of
886 column-integrated aerosol optical thickness in Beijing from AERONET
887 observations, China Particuol., 4, 330-335, DOI:
888 10.1016/s1672-2515(07)60285-1, 2006.

889 García, O. E., Díaz, J. P., Expósito, F. J., Díaz, A. M., Dubovik, O., Dubuisson,
890 P., Roger, J.-C., Eck, T. F., Sinyuk, A., Derimian, Y., Dutton, E. G., Schafer,
891 J. S., Holben, B. N., and García, C. A.: Validation of AERONET estimates
892 of atmospheric solar fluxes and aerosol radiative forcing by groundbased

893 broadband measurements, *J. Geophys. Res.*, 113, D21207,
894 <https://doi.org/10.1029/2008JD010211>, 2008.

895 García, O. E., Díaz, J. P., Expósito, F. J., Díaz, A. M., Dubovik, O., and
896 Derimian, Y.: Aerosol radiative forcing: AERONET based estimates,
897 *climate Models*, InTech, edited by: Druryan, L., ISBN: 978- 953-51-0135-2,
898 2012.

899 [Garrett, T. J., and Zhao, C.: Increased Arctic cloud longwave emissivity](#)
900 [associated with pollution from mid-latitudes, *Nature*, 440, 787-789,](#)
901 [doi:10.1038/nature04636, 2006.](#)

902 Gelencser, A.: Carbonaceous Aerosol, Atmospheric and Oceanographic
903 Sciences Libery., vol. 30. Springer, Netherland., 2004.

904 Giles, D. M., Holben, B. N., Tripathi, S. N., Eck, T. F., Newcomb, W. W.,
905 Slutsker, I., Dickerson, R. R., Thompson, A. M., Mattoo, S., Wang, S.,
906 Singh, R. P., Sinyuk, A., and Schafer, J. S.: Aerosol properties over the
907 Indo-Gangetic Plain: A mesoscale perspective from the TIGERZ
908 experiment, *J. Geophys. Res.-Atmos.*, 116(D18), DOI:
909 10.1029/2011JD015809, 2011.

910 Giles, D. M., Holben, B. N., Eck, T. F., Sinyuk, A., Smirnov, A., Slutsker, I.,
911 Dickerson, R. R., Thompson, A. M., and Schafer, J. S.: An analysis of
912 AERONET aerosol absorption properties and classifications
913 representative of aerosol source regions, *J. Geophys. Res.-Atmos.*, 117,
914 127–135, DOI: 10.1029/2012JD018127, 2012.

915 Gobbi, G. P., Kaufman, Y. J., Koren, I., and Eck, T. F.: Classification of aerosol
916 properties derived from AERONET direct sun data, *Atmos. Chem. Phys.*,
917 7, 453–458, <http://dx.doi.org/10.5194/acp-7-453-2007>, 2007

918 Goloub, P., Li, Z., Dubovik, O., Blarel, L., Podvin, T., Jankowiak, I., Lecoq, R.,
919 Deroo, C., Chatenet, B., and Morel, J. P.: PHOTONS/AERONET
920 sunphotometer network overview: description, activities, results,
921 Fourteenth International Symposium on Atmospheric and Ocean

922 Optics/Atmospheric Physics, 6936, 69360V, DOI: 10.1117/12.783171,
923 2007.

924 Haywood, J. M. and Shine, K. P.: The effect of anthropogenic sulfate and soot
925 aerosol on the clear sky planetary radiation budget, *Geophys. Res. Lett.*,
926 22, 603–606, <https://doi.org/10.1029/95GL00075>, 1995.

927 He, Q., Li, C., Geng, F., Yang, H., Li, P., Li, T., Liu, D., and Pei, Z.: Aerosol
928 optical properties retrieved from Sun photometer measurements over
929 Shanghai, China, *J. Geophys. Res.-Atmos.*, 117, D16204,
930 <https://doi.org/10.1029/2011JD017220>, 2012.

931 Holben, B. N., Eck, T. F., Slutsker, I., Tanré, D., Buis, J. P., Setzer, A., Vermote,
932 E., Reagan, J. A., Kaufman, Y. J., Nakajima, T., Lavenu, F., Jankowiak, I.,
933 and Smirnov, A.: AERONET – A Federated Instrument Network and Data
934 Archive for Aerosol Characterization, *Remote Sens. Environ.*, 66, 1–16,
935 [https://doi.org/10.1016/S0034-4257\(98\)00031-5](https://doi.org/10.1016/S0034-4257(98)00031-5), 1998.

936 Jacobson, M. Z.: A physically based treatment of elemental carbon optics:
937 implications for global direct forcing of aerosols, *Geophys. Res. Lett.*, 27,
938 217–220, DOI: 10.1029/1999gl010968, 2000.

939 Lacis, A. A. and Oinas, V.: A description of the correlated kdistribution method
940 for modeling nongray gaseous absorption, thermal emission, and multiple
941 scattering in vertically inhomogeneous atmospheres, *J. Geophys. Res.*,
942 96, 9027–9063, DOI: 10.1029/90JD01945, 1991.

943 Lee, K. H., Li, Z., Cribb, M. C., Liu, J., Wang, L., Zheng, Y., Xia, X., Chen, H.,
944 and Li, B.: Aerosol optical depth measurements in eastern China and a
945 new calibration method, *J. Geophys. Res.*, 115, 4038–4044,
946 <https://doi.org/10.1029/2009JD012812>, 2010.

947 Li, C.C., Mao, J.T., Lau, A.K.H., Chen, J.C., Yuan, Z.B., Liu, X.Y., Zhu, A.H.,
948 and Liu, G.Q.: Characteristics of distribution and seasonal variation of
949 aerosol optical depth in eastern China with MODIS products, *Chinese
950 Science Bulletin.*, 48, 2488-2495, DOI: 10.1360/03wd0224, 2003.

951 Li, Z., Chen, H., Cribb, M., Dickerson, R., Holban, B., Li, C., Lu, D., Luo, Y.,
952 Maring, H., Shi, G., Tsay, S.C., Wang, P., Wang, Y., Xia, X., and Zhao, F.:
953 Overview of the East Asian Studies on tropospheric aerosols, an
954 international regional experiment(EAST-AIRE), *J. Geophys. Res.*, 112,
955 D22S00. <http://dx.doi.org/10.1029/2007JD008853>, 2007.

956 Li, X., and Zhang, L.: Analysis of aerosol sources and optical properties based
957 on backward trajectory method over SACOL, *Acta Physica Sin.*, 61, 1-9,
958 DOI: 10.7498/aps.61.023402, 2012.

959 Li, Z. Q., Eck, T., Zhang, Y., Zhang, Y. H., Li, D. H., Li, L., Xu, H., Hou, W. Z., Lv,
960 Y., Goloub, P., and Gu, X. F.: Observations of residual submicron fine
961 aerosol particles related to cloud and fog processing during a major
962 pollution event in Beijing, *Atmos. Environ.*, 86, 187–192, DOI:
963 10.1016/j.atmosenv.2013.12.044, 2014.

964 Li, Z., Lau, W. K.-M., Ramanathan, V., Wu, G., Ding, Y., Manoj, M. G., Liu, J.,
965 Qian, Y., Li, J., Zhou, T., Fan, J., Rosenfeld, D., Ming, Y., Wang, Y., Huang,
966 J., Wang, B., Xu, X., Lee, S.- S., Cribb, M., Zhang, F., Yang, X., Takemura,
967 T., Wang, K., Xia, X., Yin, Y., Zhang, H., Guo, J., Zhai, P. M., Sugimoto, N.,
968 Babu, S. S., and Brasseur, G. P.: Aerosol and monsoon climate
969 interactions over Asia, *Rev. Geophys.*, 54, 866–929,
970 <https://doi.org/10.1002/2015RG000500>, 2016.

971 Li, Z.Q., Xu, H., Li, K. T., Li, D. H., Xie, Y. S., Li, L., Zhang, Y., Gu, X.F., Zhao,
972 W., Tian, Q.J., Deng, R.R., Su, X.L., Huang, B., Qiao, Y.L., Cui, W.Y., Hu,
973 Y., Gong, C.L., Wang, Y.Q., Wang, X.F., Wang, J.P., Du, W.B., Pan, Z.Q.,
974 Li, Z.Z., and Bu, D.: Comprehensive Study of Optical, Physical, Chemical,
975 and Radiative Properties of Total Columnar Atmospheric Aerosols over
976 China: An Overview of Sun–Sky Radiometer Observation Network
977 (SONET) Measurements, *Bulletin of the American Meteorological Society.*,
978 99(4), 739–755, <https://doi.org/10.1175/BAMS-D-17-0133.1>, 2018.

979 Luo, Y., Lu, D., Zhou, X., and Li, W.: Analyses on the spatial distribution of
980 aerosol optical depth over china in recent 30 years, *Chinese Journal of*

981 Atmospheric Sciences., 26, 721-730, DOI: 10.1002/mop.10502, 2002.

982 Mai, B., Deng, X., Xia, X., Che, H., Guo, J., Liu, X., Zhu, J., and Ling, C.:
983 Column-integrated aerosol optical properties of coarse- and fine-mode
984 particles over the Pearl River Delta region in China, *Sci. Total. Environ.*,
985 622–623, 481-492, DOI: 10.1016/j.scitotenv.2017.11.348, 2018.

986 Myhre, G.: Consistency between satellite-derived and modeled estimates of
987 the direct aerosol effect, *Science*, 325, 187-190, DOI:
988 10.1126/science.1174461, 2009.

989 Nakajima, T. and Tanaka, M.: Algorithms for radiative intensity calculations in
990 moderately thick atmospheres using a truncation approximation, *J. Quant.*
991 *Spectrosc. Ra.*, 40, 51–69,
992 [https://doi.org/10.1016/0022-4073\(88\)90031-3](https://doi.org/10.1016/0022-4073(88)90031-3), 1988.

993 Pappalardo, G., Amodeo, A., Apituley, A., Comeron, A., Freudenthaler, V.,
994 Linné, H., Ansmann, A., Bösenberg, J., D'Amico, G., Mattis, I., Mona, L.,
995 Wandinger, U., Amiridis, V., AladosArboledas, L., Nicolae, D., and
996 Wiegner, M.: EARLINET: towards an advanced sustainable European
997 aerosol lidar network, *Atmos. Meas. Tech.*, 7, 2389–2409,
998 <https://doi.org/10.5194/amt-7-2389-2014>, 2014.

999 Prats, N., Cachorro, V. E., Berjón, A., Toledano, C., and De Frutos, A. M.:
1000 Column-integrated aerosol microphysical properties from AERONET Sun
1001 photometer over southwestern Spain, *Atmos. Chem. Phys.*, 11, 12535–
1002 12547, DOI:10.5194/acp-11-12535-2011, 2011.

1003 Qin, K., Wang, L.Y., Wu, L.X., Xu, J., Rao, L.L., Letu, H., Shi, T.W., Wang, R.F.,
1004 2017. A campaign for investigating aerosol optical properties during winter
1005 hazes over Shijiazhuang, China, *Atmos. Res.*, 198, 113-122,
1006 <https://doi.org/10.1016/j.atmosres.2017.08.018>, 2017.

1007 Ramanathan, V., Crutzen, P. J., Kiehl, J. T., and Rosenfeld, D.: Aerosol,
1008 climate, and hydrological cycle, *Science* 294, 2119–2124,
1009 <https://doi.org/10.1126/science.1064034>, 2001.

1010 Remer, L. A., and Kaufman, Y. J.: Dynamic aerosol model: Urban/industrial

1011 aerosol, J. Geophys. Res., 103, 13859–13871,
1012 <https://doi.org/10.1029/98jd00994>, 1998.

1013 Roger, J. C., Mallet, M., Dubuisson, P., Cachier, H., Vermote, E., Dubovik, O.,
1014 and Despiiau, S.: A synergetic approach for estimating the local direct
1015 aerosol forcing: applications to an urban zone during the ESCOMPTE
1016 experiment, J. Geophys. Res., 111, D13208,
1017 <https://doi.org/10.1029/2005JD006361>, 2006.

1018 Russell, P. B., Bergstrom, R. W., Shinozuka, Y., Clarke, A. D., DeCarlo, P. F.,
1019 Jimenez, J. L., Livingston, J. M., Redemann, J., Dubovik, O., and Strawa,
1020 A.: Absorption Angstrom Exponent in AERONET and related data as an
1021 indicator of aerosol composition, Atmos. Chem. Phys., 10, 1155–1169,
1022 <https://doi.org/10.5194/acp-10-1155-2010>, 2010.

1023 [Shen, L., Zhao, C., Ma, Z., Li, Z., Li, J., and Wang, K.: Observed decrease of](#)
1024 [summer sea-land breeze in Shanghai from 1994 to 2014 and its](#)
1025 [association with urbanization, Atmos. Res.,](#)
1026 [doi:10.1016/j.atmosres.2019.05.007, 2019.](#)

1027 Shettle, E. P., and Fenn, R. W.: Models for the aerosols of the lower
1028 atmosphere and the effects of humidity variations on their optical
1029 properties. AFCRL Tech. Rep. 79 0214, Air Force Cambridge Research
1030 Laboratory, Hanscom Air Force Base, MA, 100 pp, 1979.

1031 Stamnes, K., Tsay, S. C., Wiscombe, W., and Jayaweera, K.: Numerically
1032 stable algorithm for discrete-ordinate-method radiative transfer in multiple
1033 scattering and emitting layered media, Appl. Optics., 27, 2502–2509,
1034 <https://doi.org/10.1364/ao.27.002502>, 1988.

1035 Su, X. L., Wang, Q., Li, Z. Q., Calvello, M., Esposito, F., Pavese, G., Lin, M. J.,
1036 Cao, J. J., Zhou, C. Y., Li, D. H., Xu, H.: Regional transport of
1037 anthropogenic pollution and dust aerosols in spring to Tianjin — A coastal
1038 megacity in China, Sci. Total Environ., 584-585, 381-392,
1039 <https://doi.org/10.1016/j.scitotenv.2017.01.016>, 2017.

1040 [Sun, J. Y., Zhang, Q., Canagaratna, M. R., Zhang, Y. M., Ng, N. L., Sun, Y. L.,](#)

1041 [Jayne, J. T., Zhang, X. C., Zhang, X. Y., and Worsnop, D. R.: Highly time-](#)
1042 [and size-resolved characterization of submicron aerosol particles in](#)
1043 [Beijing using an Aerodyne Aerosol Mass Spectrometer, Atmos. Environ.,](#)
1044 [44, 131–140, 2010.](#)

1045 [Sun, T., Che, H., Qi, B., Wang, Y., Dong, Y., Xia, X., Wang, H., Gui, K., Zheng,](#)
1046 [Y., Zhao, H., Ma, Q., Du, R., and Zhang, X.: Aerosol optical characteristics](#)
1047 [and their vertical distributions under enhanced haze pollution events:](#)
1048 [effect of the regional transport of different aerosol types over eastern](#)
1049 [China, Atmos. Chem. Phys., 18, 2949–2971,](#)
1050 <https://doi.org/10.5194/acp-18-2949-2018>, 2018.

1051 Takamura, T., and Nakajima, T.: Overview of SKYNET and its activities, Opt.
1052 Pura Apl., 37, 3303–3308, 2004.

1053 Tao, R., Che, H. Z., Chen, Q. L., Wang, Y. Q., Sun, J. Y., Zhang, X. C., Lu, S.,
1054 Guo, J. P., Wang, H., and Zhang, X.Y.: Development of an integrating
1055 sphere calibration method for Cimel sunphotometers in China aerosol
1056 remote sensing network, Particuology 13, 88–99.
1057 <https://doi.org/10.1016/j.partic.2013.04.009>, 2014.

1058 Twomey, S. A., Piepgrass, M., and Wolfe, T. L.: An assessment of the impact of
1059 pollution on the global cloud albedo, Tellus, 36B, 356–366,
1060 <https://doi.org/10.1111/j.1600-0889.1984.tb00254.x>, 1984.

1061 Wan, X., Kang, S.C., Wang, Y.S., Xin, J.Y., Liu, B., Guo, Y.H., Wen, T.X., Zhang,
1062 G.S., and Cong, Z.Y.: Size distribution of carbonaceous aerosols at a
1063 high-altitude site on the central Tibetan Plateau (Nam Co Station, 4730m
1064 a.s.l.), Atmos. Res., 153, 155–164,
1065 <https://doi.org/10.1016/j.atmosres.2014.08.008>, 2015.

1066 Wang, X., Huang, J.P., Ji, M.X., and Higuchi, K.: Variability of east Asia dust
1067 events and their long-term trend, Atmos. Environ., 42, 3156–3165,
1068 <http://dx.doi.org/10.1016/j.atmosenv.2007.07.046>, 2007.

1069 Wang, L. C., Gong, W., Xia, X. A., Zhu, J., Li, J., and Zhu, Z. M.: Long-term
1070 observations of aerosol optical properties at Wuhan, an urban site in

1071 Central China, Atmos. Environ., 101, 94–102, DOI:
1072 10.1016/j.atmosenv.2014.11.021, 2015.

1073 Wang, P., Che, H. Z., Zhang, X. C., Song, Q. L., Wang, Y. Q., Zhang, Z. H., Dai,
1074 X., and Yu, D. J.: Aerosol optical properties of regional background
1075 atmosphere in Northeast China, Atmos. Environ., 44, 4404–4412, DOI:
1076 10.1016/j.atmosenv.2010.07.043 , 2010.

1077 Wang, Z., Liu, D., Wang, Y., Wang, Z., and Shi, G.: Diurnal aerosol variations
1078 do affect daily averaged radiative forcing under heavy aerosol loading
1079 observed in Hefei, China, Atmos. Meas. Tech., 8, 2901–2907,
1080 <https://doi.org/10.5194/amt-8-2901-2015>, 2015.

1081 Wehrli, C.: Calibration of filter radiometers for the GAW Aerosol Optical Depth
1082 network at Jungfraujoch and Mauna Loa, in: Proceedings of ARJ
1083 Workshop, SANW Congress, Davos, Switzerland, 70–71, 2002.

1084 Whitey, K. T.: The physical characteristics of sulfur aerosols. Atmos. Environ.,
1085 41(supp-S), 25-49, DOI: 10.1016/j.atmosenv.2007.10.057, 1978.

1086 Wu, Y.F., Zhang, R.J., Pu, Y.F., Zhang, L.M., Ho, K.F., and Fu, C.B.: Aerosol
1087 optical properties observed at a semi-arid rural site in Northeastern China,
1088 Aerosol. Air. Qual. Res., 12,503–514, DOI: 10.4209/aaqr.2011.11.0202 ,
1089 2012.

1090 [Xia, C., Sun, J. Y., Qi, X. F., Shen, X. J., Zhong, J. T., Zhang, X. Y., Wang, Y. Q.,](#)
1091 [Zhang, Y. M., and Hu, X. Y.: Observational study of aerosol hygroscopic](#)
1092 [growth on scattering coefficient in Beijing: A case study in March of 2018,](#)
1093 [Sci. Total Environ., 685, 239-247, 2019.](#)

1094 Xia, X.: A closer looking at dimming and brightening in China during 1961–
1095 2005, Ann. Geophys., 28, 1121–1132, doi:10.5194/angeo-28-1121-2010,
1096 2010.

1097 Xia, X., Chen, H., Goloub, P., Zong, X., Zhang, W., and Wang, P.:
1098 Climatological aspects of aerosol optical properties in North China Plain
1099 based on ground and satellite remote-sensing data, J. Quant. Spectrosc.
1100 Ra., 127, 12–23, DOI: 10.1016/j.jqsrt.2013.06.024, 2013.

1101 Xie, C., Nishizawa, T., Sugimoto, N., Matsui, I., and Wang, Z.: Characteristics
1102 of aerosol optical properties in pollution and Asian dust episodes over
1103 Beijing, China. *Appl. Opt.*, 47, 4945-4951, DOI: 10.1364/AO.47.004945,
1104 2008.

1105 [Xie, S., Liu, X., Zhao, C., and Zhang, Y.: Sensitivity of CAM5-Simulated Arctic](#)
1106 [Clouds and Radiation to Ice Nucleation Parameterization, *J. Climate.*, 26,](#)
1107 [5981-5999, doi:10.1175/jcli-d-12-00517.1, 2013.](#)

1108 Xin, J., Wang Y, Li, Z.Q., Wang, P.C., Hao, W.M., Nordgren, B.L., Wang, S.G.,
1109 Liu, G.R., Wang, L.L., Wen, T.X., Sun, Y., and Hu, B.: Aerosol optical
1110 depth (AOD) and Ångström exponent of aerosols observed by the
1111 Chinese Sun Hazemeter Network from August 2004 to September 2005, *J.*
1112 *Geophys. Res.*, 112, D05203, DOI: 10.1029/2006JD007075, 2007

1113 Xin, J.Y., Wang, L.L., Wang, Y.S., Li, Z., and Wang, P.: Trends in aerosol
1114 optical properties over the Bohai Rim in Northeast China from 2004 to
1115 2010, *Atmos. Environ.*, 45, 6317–6325, DOI:
1116 10.1016/j.atmosenv.2011.08.052, 2011.

1117 Xin J, Wang Y, Pan Y, Ji, D., Liu, Z., Wen, T.X., Wang, Y.H., Li, X.R., Sun, Y.,
1118 Sun, J., Wang, P.C., Wang, G.H., Wang, X.M., Cong, Z.Y., Song, T., Hu, B.,
1119 Wang, L.L., Tang, G.Q., Gao, W.K., Guo, Y.H., Miao, H.Y., Tian, S.L., and
1120 Wang, L.: The campaign on atmospheric aerosol research network of
1121 China: CARE-China, *Bulletin of the American Meteorological Society.*, 96,
1122 1137-1155, <https://doi.org/10.1175/BAMS-D-14-00039.1>, 2015.

1123 [Yang, X., Zhao, C., Zhou, L., Li, Z., Cribb, M., and Yang, S.: Wintertime cooling](#)
1124 [and a potential connection with transported aerosols in Hong Kong during](#)
1125 [recent decades, *Atmos. Res.*, 211, 52–61,](#)
1126 [doi:10.1016/j.atmosres.2018.04.029, 2018.](#)

1127 [Yang, X., Zhao, C., Zhou, L., Wang, Y., and Liu, X.: Distinct impact of different](#)
1128 [types of aerosols on surface solar radiation in China, *J. Geophys.*](#)
1129 [Res.-Atmospheres,](#) 121, 6459–6471. DOI:
1130 <https://doi.org/10.1002/2016jd024938>, 2016.

1131 [Yang, Y., Zhao, C., Dong, X., Fan, G., Zhou, Y., Wang, Y., Zhao, L., Lv, F., and](#)
1132 [Yan, F.: Toward understanding the process-level impacts of aerosols on](#)
1133 [microphysical properties of shallow cumulus cloud using aircraft](#)
1134 [observations, Atmos. Res., doi:10.1016/j.atmosres.2019.01.027, 2019.](#)

1135 [Yang, Y., Zhao, C., Sun, L., and Wei, J.: Improved aerosol retrievals over](#)
1136 [complex regions using NPP Visible Infrared Imaging Radiometer Suite](#)
1137 [observations, Earth. Space. Sci., doi:10.1029/2019ea000574, 2019.](#)

1138 Yuan, Y., Shuai, Y., Li, X.W., Liu, B., and Tan, H.P.: Using a new aerosol
1139 relative optical thickness concept to identify aerosol particle species,
1140 Atmos. Res., 150, 1–11, DOI: 10.1016/j.atmosres.2014.07.007, 2014.

1141 [Zhang, L., Sun, J. Y., Shen, X. J., Zhang, Y. M., Che, H., Ma, Q. L., Zhang, Y.](#)
1142 [W., Zhang, X. Y., and Ogren, J. A.: Observations of relative humidity](#)
1143 [effects on aerosol light scattering in the Yangtze River Delta of China,](#)
1144 [Atmos. Chem. Phys., 15, 8439-8454,](#)
1145 <https://doi.org/10.5194/acp-15-8439-2015>, 2015.

1146 Zhang, M., Ma, Y., Gong, W., Liu, B., Shi, Y., and Chen, Z.: Aerosol optical
1147 properties and radiative effects: Assessment of urban aerosols in central
1148 China using 10-year observations, Atmos. Environ., 182, 275-285, DOI:
1149 10.1016/j.atmosenv.2018.03.040, 2018

1150 Zhang, R., Jing, J., Tao, J., Hsu, S.-C., Wang, G., Cao, J., Lee, C.S.L., Zhu, L.,
1151 Chen, Z., Zhao, Y., and Shen, Z.: Chemical characterization and source
1152 apportionment of PM_{2.5} in Beijing: seasonal perspective, Atmos. Chem.
1153 Phys., 13, 7053–7074, <http://dx.doi.org/10.5194/acp-13-7053-2013>, 2013

1154 [Zhao, C., and Garrett, T. J.: Effects of Arctic haze on surface cloud radiative](#)
1155 [forcing, Geophys. Res. Lett., 42, 557–564. doi:10.1002/2014gl062015,](#)
1156 [2015.](#)

1157 [Zhao, C., Lin, Y., Wu, F., Wang, Y., Li, Z., Rosenfeld, D., and Wang, Y.:](#)
1158 [Enlarging Rainfall Area of Tropical Cyclones by Atmospheric Aerosols,](#)
1159 [Geophys. Res. Lett., doi:10.1029/2018gl079427, 2018.](#)

1160 [Zhao, C., Wang, Y., Shi, X., Zhang, D., Wang, C., Jiang, J. H., Zhang, Q., and](#)

1161 [Fan, H.: Estimating the contribution of local primary emissions to](#)
1162 [particulate pollution using high-density station observations, J. Geophys.](#)
1163 [Res.-Atmospheres, doi:10.1029/2018jd028888, 2019.](#)

1164 Zhao, H., Che, H., Ma, Y., Xia, X., Wang, Y., Wang, P., and Wu, X.: Temporal
1165 variability of the visibility, particulate matter mass concentration and
1166 aerosol optical properties over an urban site in Northeast China, Atmos.
1167 Res., 166, 204–212, DOI: 10.1016/j.atmosres.2015.07.003, 2015.

1168 Zhao H., Che H., Wang Y., Wang H., Ma Y., and Wang Y.: Investigation of the
1169 Optical Properties of Aerosols over the Coastal Region at Dalian,
1170 Northeast China, Atmosphere., 7(8), 103, DOI: 10.3390/atmos7080103,
1171 2016

1172 Zhao, H., Che, H., Xia, X., Wang, Y., Wang, H., Wang, P., Ma, Y., Yang, H., Liu,
1173 Y., Wang, Y., Gui, K., Sun, T., Zheng, Y., and Zhang, X.: Multi-year
1174 ground-based measurements of aerosol optical properties and direct
1175 radiative effect over different surface types in northeastern China, J.
1176 Geophys. Res.-Atmos., 123, 13,887–13,916,
1177 <https://doi.org/10.1029/2018JD029141>, 2018

1178 [Zhang, K., Zhao, C., Fan, H., Yang, Y., and Sun, Y.: Toward Understanding the](#)
1179 [Differences of PM2.5 Characteristics Among Five China Urban Cities,](#)
1180 [Asia-Pac. J. Atmos. Sci., doi:10.1007/s13143-019-00125-w, 2019.](#)

1181 [Zheng, C., Zhao, C., Zhu, Y., Wang, Y., Shi, X., Wu, X., Chen, T., Wu, F., and](#)
1182 [Qiu, Y.: Analysis of influential factors for the relationship between PM2.5](#)
1183 [and AOD in Beijing, Atmos. Chem. Phys., 17, 13473–13489, doi:](#)
1184 [10.5194/acp-17-13473-2017, 2017.](#)

1185 [Zheng, Y., Che, H., Xia, X., Wang, Y., Wang, H., Wu, Y., Tao, J., Zhao, H., An,](#)
1186 [L., Li, L., Gui, K., Sun, T., Li, X., Sheng, Z., Liu, C., Yang, X., Liang, Y.,](#)
1187 [Zhang, L., Kuang, X., Luo, S., and You, Y.: Five-year observation of](#)
1188 [aerosol optical properties and its radiative effects to planetary boundary](#)
1189 [layer during air pollution episodes in North China: Intercomparison of a](#)
1190 [plain site and a mountainous site in Beijing, Sci. Total. Environ., 674,](#)

1191 | [140-158, 2019.](#)
1192 | Zhu, J., Che, H., Xia, X., Chen, H. B., Goloub, P., and Zhang, W.:
1193 | Column-integrated aerosol optical and physical properties at a regional
1194 | background atmosphere in North China Plain, Atmos. Environ., 84, 54–64,
1195 | DOI: 10.1016/j.atmosenv.2013.11.019, 2014.
1196 | Zhuang, B., Wang, T., Li, S., Liu, J., Talbot, R., Mao, H., Yang, X., Fu, C., Yin,
1197 | C., Zhu, J., Che, H., and Zhang, X.: Optical properties and radiative
1198 | forcing of urban aerosols in Nanjing over China, Atmos. Environ., 83, 43–
1199 | 52, DOI: 10.1016/j.atmosenv.2013.10.052, 2014.

1200 |
1201 |
1202 |
1203 |

1204 | **Figure captions**

1205 | **Figure 1. Annual spatial distribution of aerosol volume-size distributions**
1206 | **at the CARSNET sites**

1207 | **Figure 2. Annual spatial distribution of aerosol optical depth (AOD) at 440**
1208 | **nm at the CARSNET sites**

1209 | **Figure 3. Annual spatial distribution of extinction Ångström exponent**
1210 | **(AE) 440-870 nm at the CARSNET sites**

1211 | **Figure 4. Annual spatial distribution of fine mode fraction at the**
1212 | **CARSNET sites**

1213 | **Figure 5. Annual spatial distribution of the single scattering albedo (SSA)**
1214 | **at 440 nm at the CARSNET sites**

1215 | **Figure 6. Annual spatial distribution of absorption aerosol optical depth**
1216 | **(AAOD) at 440 nm at the CARSNET sites**

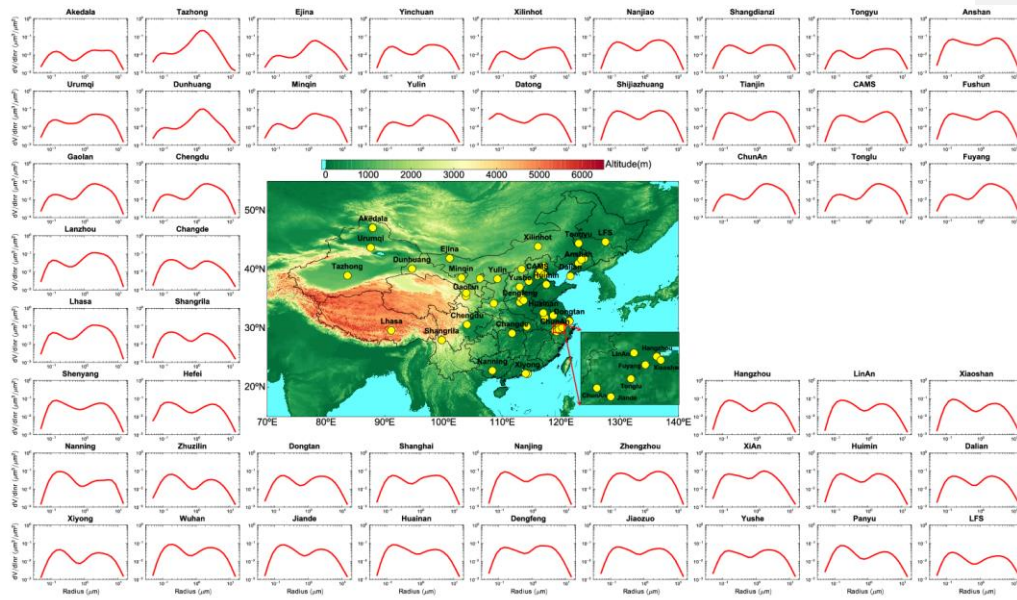
1217 | **Figure 7. Annual spatial distribution of direct aerosol radiative effect at**
1218 | **the bottom of the atmosphere at the CARSNET sites**

1219 | **Figure 8. Annual spatial distribution of direct aerosol radiative effect at**
1220 | **the top of the atmosphere at the CARSNET sites**

1221 **Figure 9. Annual spatial distribution of the aerosol type classification of**
1222 **types I–VII at the CARSNET sites**
1223 **Table 1 The aerosol type classification based on the optical properties**
1224

1225
1226
1227

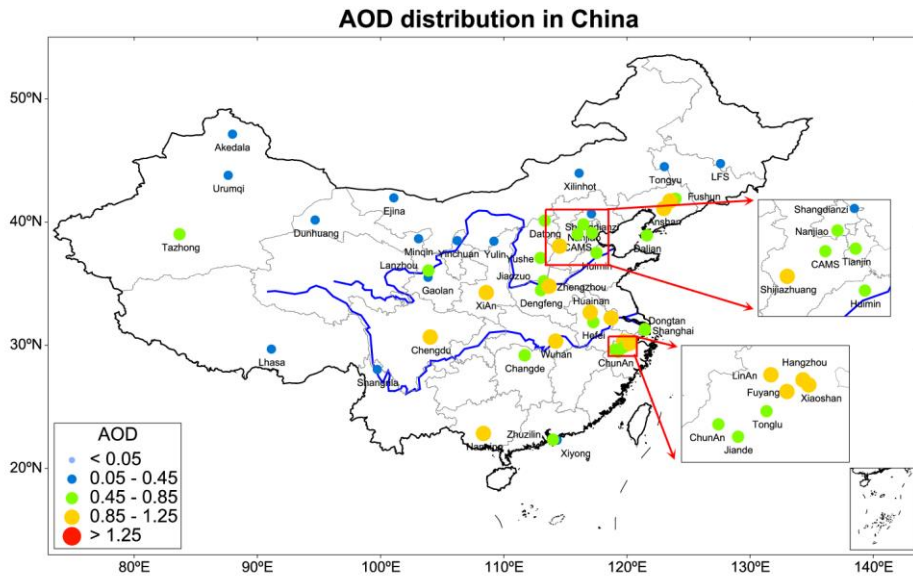
Figure 1. Annual spatial distribution of aerosol volume-size distributions at the CARSNET sites



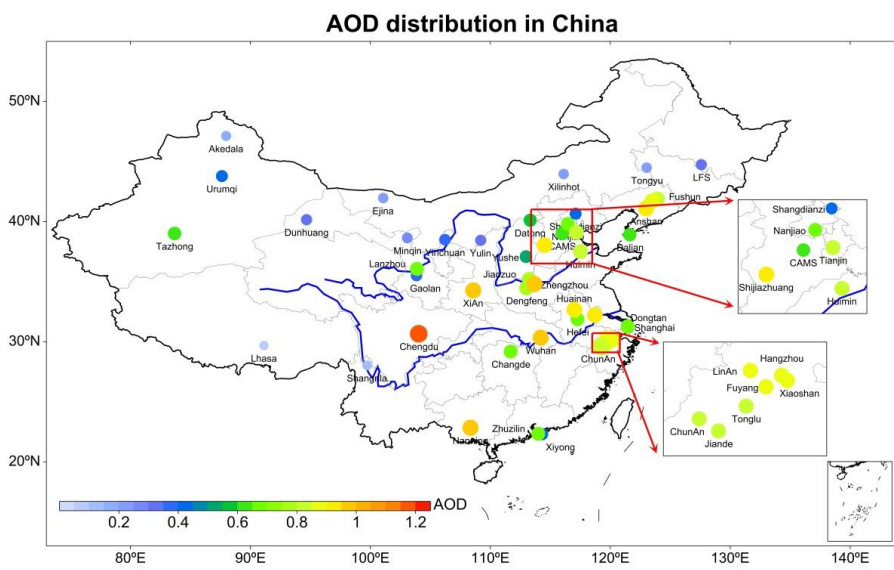
1228
1229

1230 **Figure 2. Annual spatial distribution of aerosol optical depth (AOD) at 440**
 1231 **nm at the CARSNET sites**

1232



1233

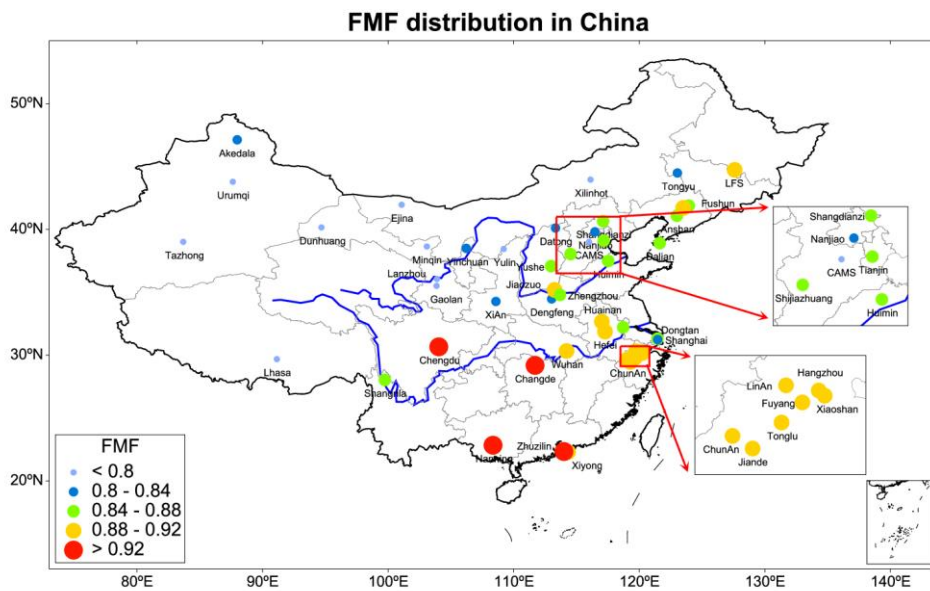


1234

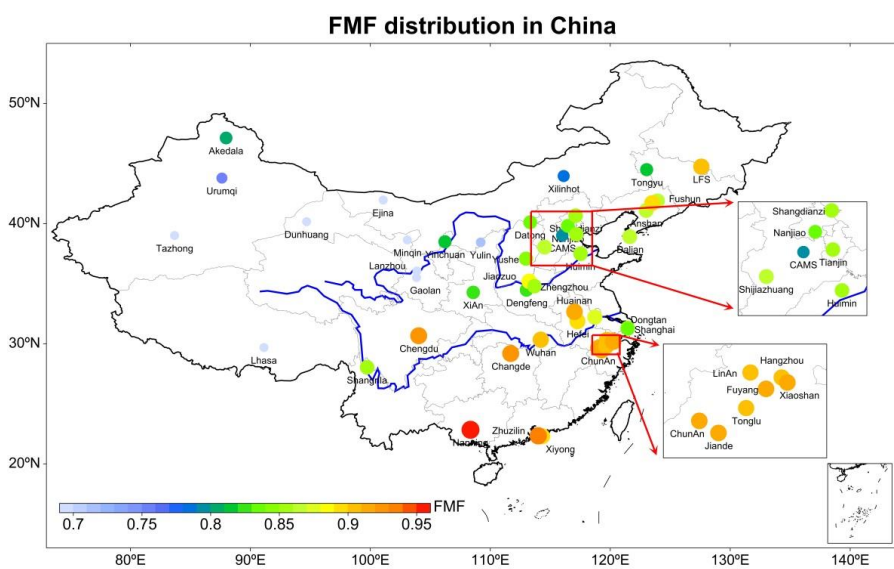
1235

1242 **Figure 4. Annual spatial distribution of fine mode fraction at the**
 1243 **CARSNET sites**

1244



1245

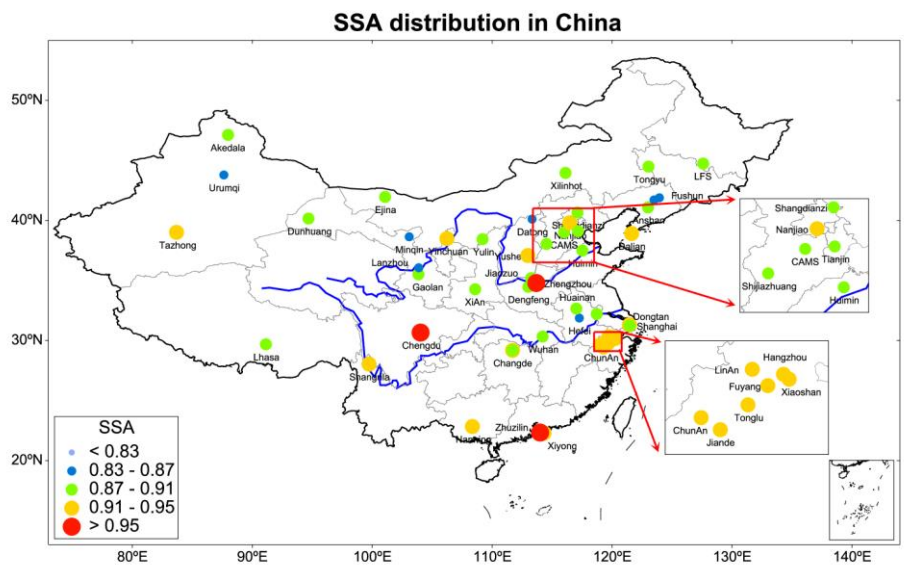


1246

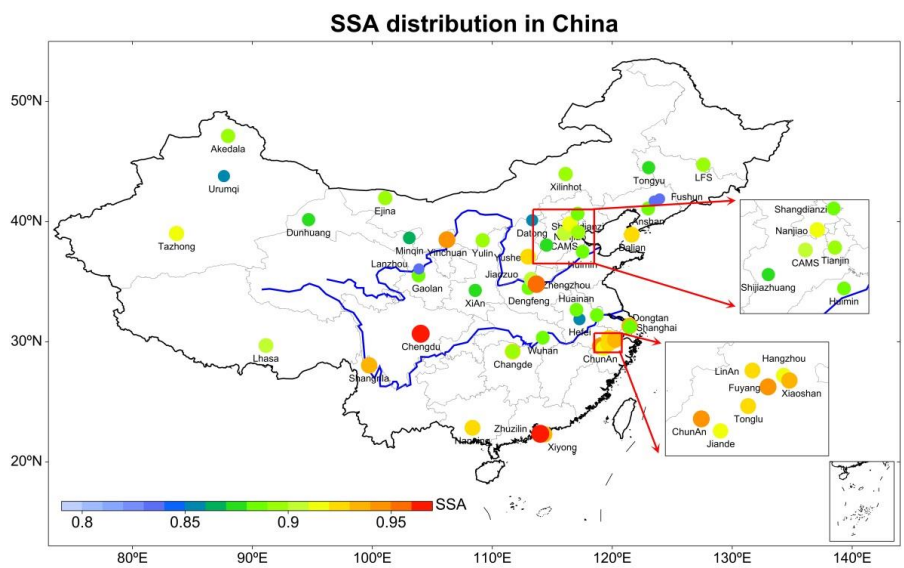
1247

1248 **Figure 5. Annual spatial distribution of the single scattering albedo (SSA)**
 1249 **at 440 nm at the CARSNET sites**

1250



1251



1252

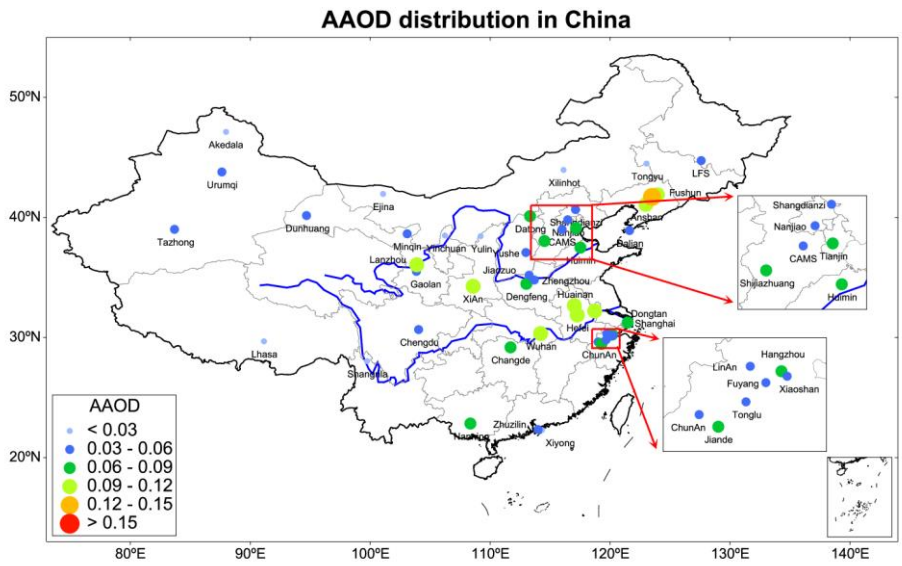
1253

1254

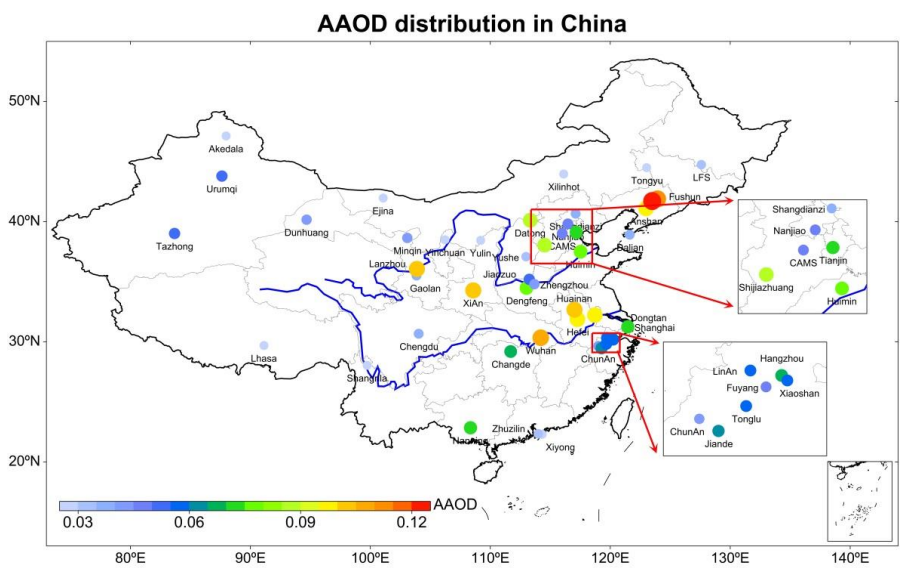
1255

1256
1257
1258

Figure 6. Annual spatial distribution of absorption aerosol optical depth (AAOD) at 440 nm at the CARSNET sites



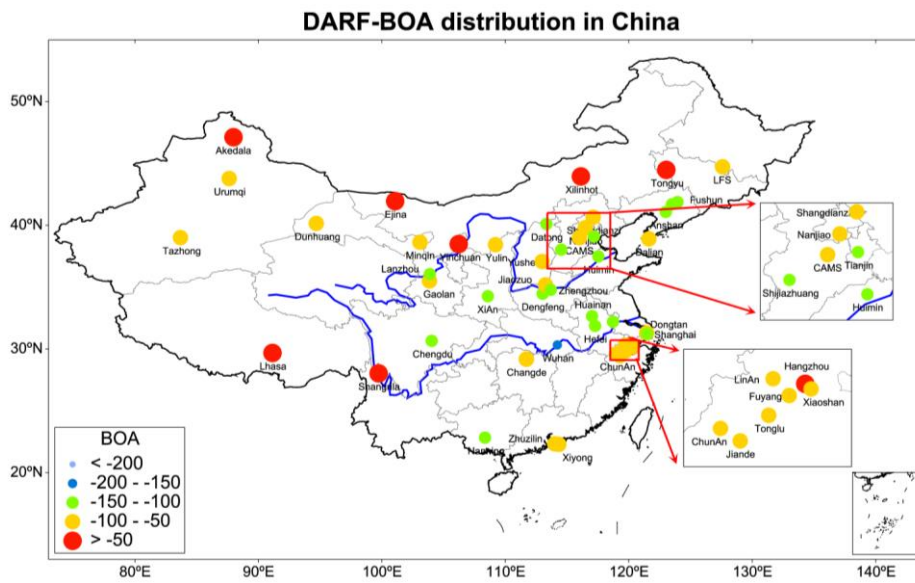
1259



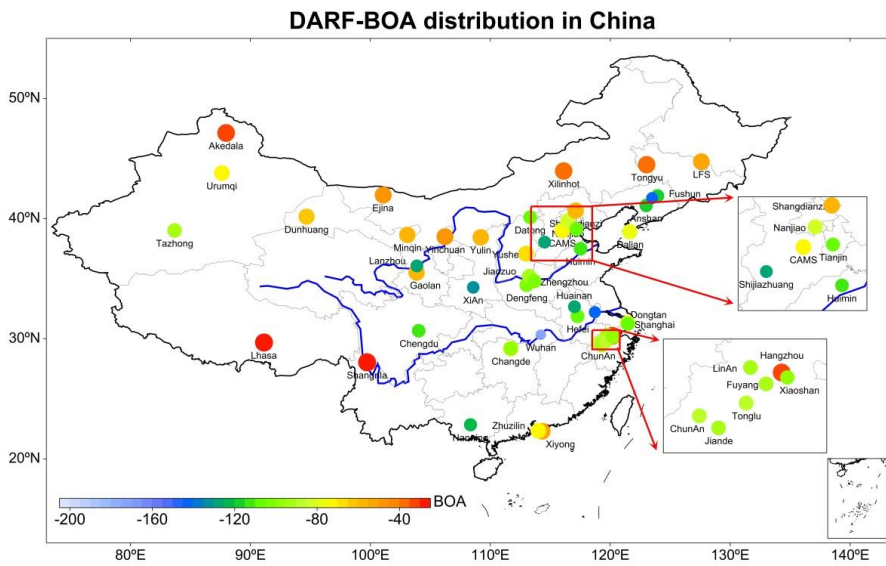
1260
1261

1262 **Figure 7. Annual spatial distribution of direct aerosol radiative effect at**
 1263 **the bottom of the atmosphere at the CARSNET sites**

1264



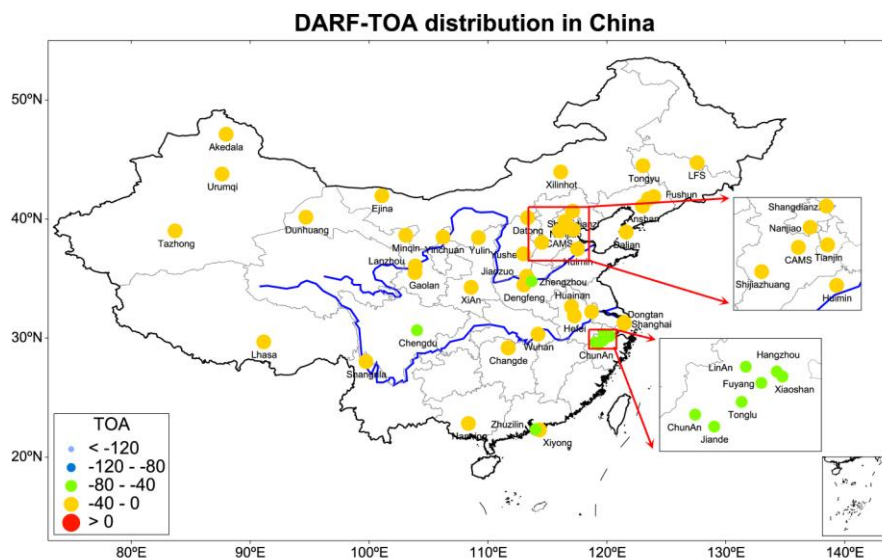
1265



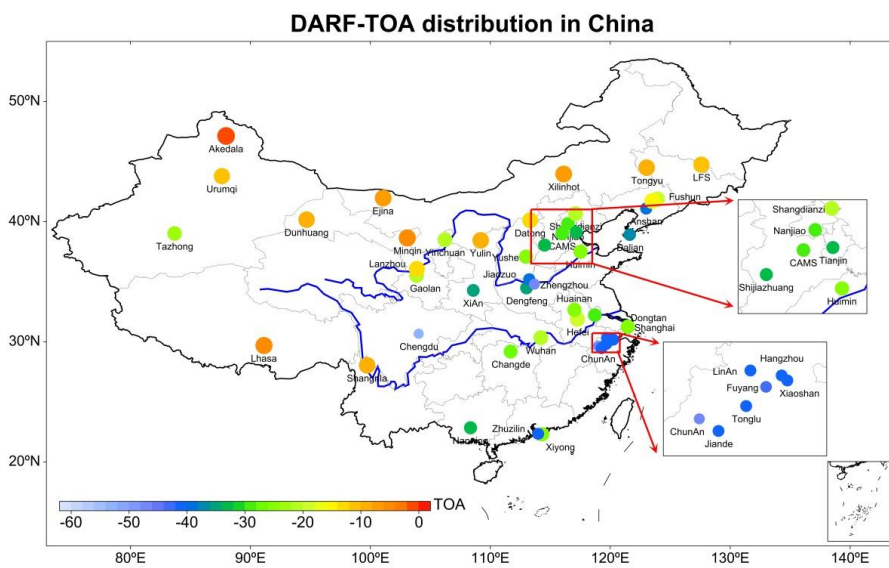
1266

1267

1268 **Figure 8. Annual spatial distribution of direct aerosol radiative effect at**
 1269 **the top of the atmosphere at the CARSNET sites**



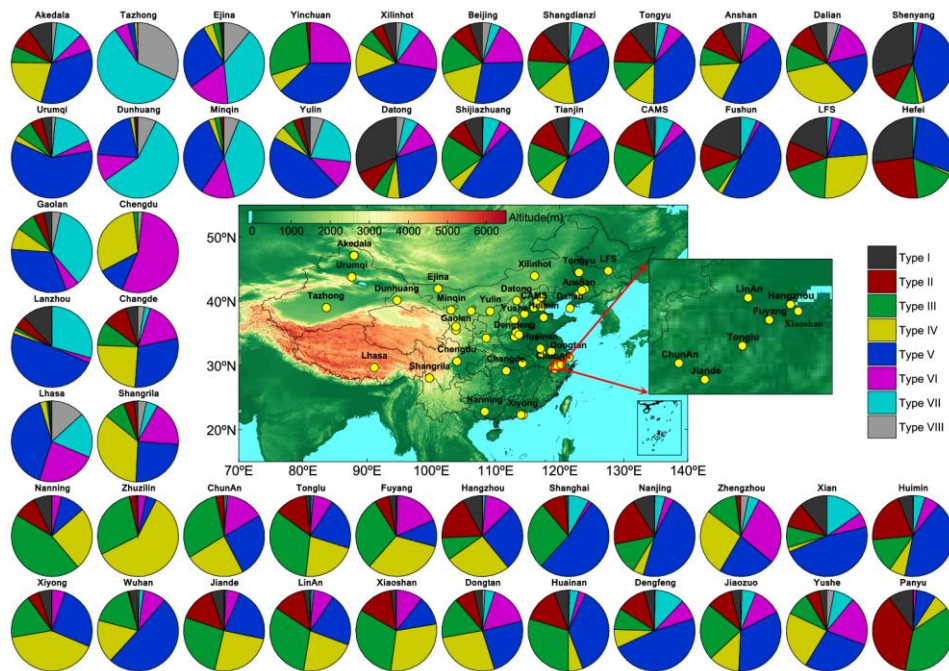
1270



1271
 1272

1273 **Figure 9. Annual spatial distribution of the aerosol type classification of**
 1274 **types I–VII at the CARSNET sites**

1275



1276
 1277

1278 **Table 1. The aerosol type classification based on the optical properties.**

1279

Type	EAE	SSA	absorbing properties and particle size
I	$EAE > 1.20$	$SSA_{440nm} \leq 0.85$	fine-mode particles with highly-absorbing
II	$EAE > 1.20$	$0.85 \leq SSA_{440nm} < 0.90$	fine-mode particles with moderately-absorbing
III	$EAE > 1.20$	$0.90 \leq SSA_{440nm} < 0.95$	fine-mode particles with slightly-absorbing
IV	$EAE > 1.20$	$SSA_{440nm} > 0.95$	fine-mode particles with weakly-absorbing
V	$0.60 \leq EAE < 1.20$	$SSA_{440nm} \leq 0.95$	mixed-absorbing particles
VI	$0.60 \leq EAE < 1.20$	$SSA_{440nm} > 0.95$	mixed-slightly absorbing particles
VII	$EAE \leq 0.60$	$SSA_{440nm} \leq 0.95$	coarse mode particles with strongly absorbing (mainly dust)
VIII	$AE \leq 0.60$	$SSA_{440nm} > 0.95$	coarse-mode particles with weakly-absorbing

1280

1281

1282

1283

1284

1285

1286

1287

1288

1289

1290

1291

1292

1293

1294

1295

1296

1297 Appendix

1298 Table 1. Site information for the 50 CARSNET sites used in this study

1299

No.	Site Name	Long.	Lat.	Alt.	Site information	Obs. Num	Period
Remote sites (three sites)							
1	Akedala	47.12	87.97	562.0	55 km west of Fuhai county, Xinjiang province, and 250–300 km southeast of Kazakestan.	947	2010-2017
2	Lhasa	29.67	91.13	3663.0	In the center of Lhasa city, Qinghai-Xizang Plateau.	437	2012-2017
3	Shangri-La	28.02	99.73	3583.0	12 km northeast of Shangri-La county, Diqing area, Yunnan province	325	2013-2017
Arid and semi-arid sites (six sites)							
4	Dunhuang	40.15	94.68	1139.0	1.5 km northeast of Dunhuang city, Gansu province; near Kumutage Desert of China	2030	2012-2017
5	Ejina	41.95	101.07	940.5	West of Inner-Mongolia Province, near Mongolia and Badanjilin desert	1970	2013-2017
6	Minqin	38.63	103.08	1367.0	In Minqin county, east to Tenggeli desert and north to Badanjilin Desert, Gansu Province	481	2013-2017
7	Tazhong	39.00	83.67	1099.4	In the middle of Taklamakan Desert, Xinjiang Province	1279	2013-2017
8	Xilinhot	43.95	116.12	1003.0	5 km southeast of Xilinhot City, near Hunshandake sand-land, Inner-Mongolia Province,	1464	2013-2017
9	Tongyu	44.42	122.87	151.0	In Tonyu city, west of Jilin Province	817	2010-2011
Rural sites on the Chinese Loess Plateau or nearby (three sites)							
10	Mt.Gaolan	36.00	103.85	2161.6	5 km north of Lanzhou city in Gansu province	769	2015-2016
11	Yulin	38.43	109.20	1135.0	10 km north of Yulin city in Shaanxi province	716	2010-2016
12	Datong	40.10	113.33	1067.3	9 km of Datong City, but within area of rapid urbanization, Shanxi Province	914	2014-2017
Rural sites in eastern China (15 sites)							
13	Changde	29.17	111.70	565.0	18 km northwest from Changde city, Hunan province.	344	2013-2016
14	Dongtan	31.52	121.96	10.0	In the Chongmin Island, 30km east of Shanghai city	986	2012-2016
15	ChunAn	29.61	119.05	171.4	151 km southwest from Hangzhou city, Zhejiang province.	1286	2011-2015
16	Huimin	37.48	117.53	11.7	100 km Northeast of Jinan City, Shandong Province	2243	2009-2017
17	Lin'an	30.30	119.73	138.6	150 km northeast of Shanghai, and 50 km west of Hangzhou city, Zhejiang province	1834	2011-2015
18	Mt.Longfeng	44.73	127.60	330.5	In Wuchang county, 175 km northeast of Harbin city, Heilongjiang Province	1515	2012-2016
19	Fuyang	30.07	119.95	17.0	44.1 km southwest from Hangzhou city, Zhejiang province.	710	2014-2015
20	Shangdianzi	40.65	117.12	293.0	In Miyun county, 150 km northeast to Beijing city.	1520	2014-2017
21	Yushe	37.07	112.98	1041.5	1.5 km east of Yushe city in Shanxi Province	1479	2013-2017
22	Dengfeng	34.46	113.02	350.0	75 km Southwest of Zhengzhou City, Henan Province	712	2013
23	Huainan	32.65	117.02	52.0	In the central of Hefei City, Anhui Province	794	2014-2015
24	Jiande	29.45	119.28	89.0	In the southwest from Hangzhou city, Zhejiang province.	1550	2011-2015
25	Tonglu	29.80	119.64	46.1	100 km northwest from Hangzhou city, Zhejiang province.	1717	2011-2015
26	Xiaoshan	30.16	120.25	14.0	In the south of Hangzhou city, Zhejiang province.	600	2014-2015
27	Xiyong	22.28	114.33	155.2	In the eastern of Shenzhen city, Guangdong province.	189	2016
Urban sites (23 sites)							
28	Anshan	41.08	123.00	23.0	In Anshan city, central Liaoning province	193	2009-2013
29	Beijing-Nanjiao	39.80	116.47	31.3	In the southeast Beijing at city margin	1732	2014-2017
30	Beijing-CAMS	39.93	116.32	106.0	Chinese Academy of Meteorological Sciences in Beijing	1113	2012-2018
31	Chengdu	30.65	104.03	496.0	In Chengdu city, Sichuan province.	55	2014-2015
32	Dalian	38.90	121.63	91.5	Southeast coastal city in Liaoning Province	736	2012-2015
33	Fushun	41.88	123.95	80.0	In Fushun city, central Liaoning province.	231	2009-2013
34	Hangzhou	30.23	120.17	42.0	In Hangzhou city, Zhejiang province.	1663	2011-2015

35	Hefei	31.98	116.38	92.0	In Hefei city, Anhui province.	197	2016
36	Jiaozuo	35.18	113.25	113.0	In the center of Jiaozuo city, Henan province.	981	2016-2017
37	Lanzhou	36.05	103.88	1517.3	In Lanzhou city, Gansu province.	1493	2013-2017
38	Nanjing	32.05	118.77	99.3	In Nanjing city, Jiangsu province	1258	2007-2015
39	Nanning	22.82	108.35	172.0	In Nanning city, Guangxi province	286	2013-2017
40	Panyu	23	113.35	145.0	In district of Guangzhou city, Guangdong Province	436	2012-2016
41	Shanghai	31.22	121.55	14.0	In Pudong district of Shanghai city	144	2016
42	Shenyang	41.77	123.50	60.0	In Shenyang city, central Liaoning province.	541	2009-2013
43	Tianjin	39.10	117.17	3.3	Northern coastal city in North China Plain	1705	2013-2017
44	Urumqi	43.78	87.62	935.0	In Urumqi city, Xijiang province	1411	2012-2017
45	Xi'an	34.43	108.97	363.0	20 km north of center of Xian city, but within Jing River Industrial District, Shaanxi province	652	2012-2016
46	Yinchuan	38.48	106.22	1111.5	In Yinchuan city, Ningxia province.	124	2017
47	Zhengzhou	34.78	113.68	99.0	In Zhengzhou city, Henan province.	1485	2013-2017
48	Shijiazhuang	38.03	114.53	75.0	In the center of Shijiazhuang city, Hebei province.	1178	2015-2017
49	Wuhan	30.32	114.21	30	In the center of Wuhan city, Hubei province	220	2008
50	Zhuzilin	22.32	114.00	63.0	In the central of Shenzhen city, Guangdong province.	915	2010-2017

1300

1301

1302

1303

1304

1305

1306

1307

1308

1309

1310

1311

1312

1313

1314

1315

1316

1317

1318

1319

1320

1321

1322

Table 2. Annual data for aerosol microphysical properties, optical and direct radiative parameters

No.	Site	^a ReffT	^a ReffF	^a ReffC	^a VolT	^a VolF	^a VolC	^a AODt	^b Alpha	^a FMF	^a SSAT	^a Image	^a Real	^a AAOD	^a BOA	^a TOA
Remote sites (3 sites)																
1	Akedala	0.36	0.14	2.45	0.06	0.02	0.04	0.17	1.13	0.81	0.90	0.0117	1.4540	0.02	-33.65	-0.42
2	Lhasa	0.64	0.13	2.26	0.05	0.01	0.04	0.10	0.77	0.66	0.90	0.0106	1.5541	0.01	-22.13	-5.04
3	Shangri-La	0.39	0.14	2.33	0.03	0.01	0.02	0.10	1.19	0.85	0.93	0.0086	1.4626	0.01	-17.43	-8.93
	Average	0.47	0.14	2.35	0.05	0.01	0.03	0.12	1.03	0.77	0.91	0.0103	1.4902	0.01	-24.40	-4.79
Arid and semi-arid sites (6 sites)																
4	Dunhuang	0.62	0.14	1.52	0.15	0.02	0.13	0.33	0.48	0.44	0.88	0.0103	1.5491	0.04	-63.61	-8.96
5	Ejina	0.56	0.14	1.78	0.11	0.02	0.09	0.24	0.64	0.52	0.89	0.0116	1.5265	0.03	-47.66	-7.20
6	Minqin	0.56	0.13	1.87	0.13	0.02	0.11	0.30	0.68	0.59	0.86	0.0145	1.5430	0.04	-59.83	-5.01
7	Tazhong	0.71	0.14	1.38	0.30	0.03	0.27	0.60	0.25	0.35	0.92	0.0054	1.5257	0.05	-91.20	-23.49
8	Xilinhot	0.48	0.13	2.45	0.08	0.02	0.05	0.21	1.03	0.78	0.89	0.0139	1.5183	0.02	-37.14	-7.47
9	Tongyu	0.39	0.13	2.36	0.07	0.02	0.05	0.23	1.16	0.82	0.88	0.0179	1.5377	0.03	-39.13	-8.87
	Average	0.55	0.14	1.89	0.14	0.02	0.12	0.32	0.71	0.58	0.89	0.0123	1.5334	0.03	-56.43	-10.17
Rural sites on the Chinese Loess Plateau or nearby (3 sites)																
10	Mt.Gaolan	0.58	0.14	2.03	0.16	0.03	0.13	0.36	0.81	0.64	0.89	0.0108	1.5154	0.04	-59.36	-20.87
11	Yulin	0.53	0.15	2.05	0.11	0.03	0.08	0.32	0.84	0.72	0.89	0.0122	1.5070	0.03	-56.81	-9.09
12	Datong	0.35	0.13	2.15	0.19	0.09	0.10	0.58	1.15	0.83	0.86	0.0171	1.4905	0.09	-107.86	-13.71
	Average	0.49	0.14	2.08	0.15	0.05	0.10	0.42	0.93	0.73	0.88	0.0134	1.5043	0.05	-74.67	-14.56
Rural sites in eastern China (15 sites)																
13	Changde	0.32	0.16	2.18	0.14	0.07	0.07	0.58	1.15	0.88	0.93	0.0101	1.4619	0.04	-75.33	-31.44
14	Dongtan	0.37	0.16	2.12	0.17	0.08	0.09	0.62	1.21	0.86	0.93	0.0080	1.4624	0.04	-79.41	-33.18
15	ChunAn	0.30	0.18	2.30	0.19	0.12	0.08	0.81	1.22	0.92	0.94	0.0066	1.4095	0.04	-86.49	-46.48
16	Huimin	0.36	0.15	2.07	0.22	0.10	0.12	0.83	1.14	0.86	0.89	0.0147	1.4852	0.08	-111.58	-25.49

17	Lin'an	0.29	0.17	2.24	0.21	0.12	0.09	0.87	1.29	0.91	0.93	0.0089	1.4172	0.06	-93.09	-41.73
18	Mt.Longfeng	0.28	0.15	2.44	0.08	0.04	0.04	0.34	1.38	0.90	0.89	0.0165	1.4647	0.03	-51.17	-11.34
19	Fuyang	0.29	0.17	2.28	0.21	0.13	0.09	0.89	1.31	0.92	0.94	0.0070	1.4147	0.05	-91.69	-42.29
20	Shangdianzi	0.40	0.15	2.33	0.12	0.05	0.07	0.43	1.17	0.86	0.89	0.0148	1.4840	0.04	-59.99	-20.58
21	Yushe	0.41	0.15	2.18	0.14	0.06	0.08	0.50	1.07	0.84	0.92	0.0090	1.4878	0.03	-66.72	-25.99
22	Dengfeng	0.39	0.15	2.03	0.23	0.09	0.13	0.79	1.02	0.83	0.89	0.0131	1.4782	0.08	-104.78	-35.84
23	Huainan	0.30	0.17	2.25	0.21	0.13	0.08	0.91	1.17	0.92	0.88	0.0166	1.4308	0.10	-129.17	-24.44
24	Jiande	0.29	0.17	2.18	0.20	0.12	0.08	0.84	1.34	0.91	0.92	0.0099	1.4085	0.06	-91.06	-40.07
25	Tonglu	0.29	0.17	2.20	0.20	0.12	0.08	0.83	1.31	0.91	0.93	0.0091	1.4269	0.06	-89.82	-41.28
26	Xiaoshan	0.28	0.17	2.24	0.22	0.13	0.09	0.87	1.35	0.91	0.93	0.0082	1.4134	0.06	-95.23	-40.39
27	Xiyong	0.33	0.16	2.43	0.11	0.06	0.05	0.41	1.32	0.89	0.94	0.0074	1.4072	0.02	-53.18	-25.45
	Average	0.33	0.16	2.23	0.18	0.09	0.08	0.70	1.23	0.89	0.92	0.0107	1.4435	0.05	-85.25	-32.40

Urban sites (23 sites)

28	Anshan	0.36	0.17	2.24	0.26	0.12	0.14	0.94	1.12	0.86	0.89	0.0158	1.4759	0.10	-117.99	-39.66
29	Beijing-Nanjiao	0.45	0.15	2.33	0.19	0.07	0.12	0.65	1.12	0.84	0.92	0.0100	1.4939	0.05	-82.06	-29.43
30	Beijing-CAMS	0.50	0.16	2.37	0.19	0.07	0.12	0.65	1.12	0.79	0.90	0.0115	1.5108	0.05	-72.66	-29.10
31	Chengdu	0.34	0.21	2.26	0.26	0.16	0.10	1.17	1.12	0.92	0.97	0.0033	1.4116	0.04	-110.42	-52.21
32	Dalian	0.35	0.16	2.24	0.16	0.08	0.09	0.62	1.22	0.87	0.93	0.0095	1.4584	0.04	-75.50	-37.42
33	Fushun	0.38	0.17	2.34	0.22	0.09	0.12	0.80	1.12	0.87	0.84	0.0244	1.4954	0.11	-116.91	-19.59
34	Hangzhou	0.30	0.17	2.21	0.22	0.12	0.10	0.87	1.30	0.90	0.91	0.0109	1.4337	0.07	-31.57	-40.16
35	Hefei	0.29	0.15	2.37	0.18	0.10	0.08	0.69	1.28	0.90	0.85	0.0195	1.4253	0.10	-105.83	-19.22
36	Jiaozuo	0.35	0.16	2.17	0.20	0.10	0.10	0.76	1.14	0.88	0.91	0.0105	1.4722	0.05	-92.29	-39.35
37	Lanzhou	0.54	0.14	2.04	0.28	0.06	0.22	0.66	0.81	0.66	0.83	0.0197	1.5193	0.10	-126.17	-13.81
38	Nanjing	0.33	0.16	2.16	0.25	0.12	0.12	0.94	1.13	0.88	0.88	0.0154	1.4446	0.10	-143.38	-28.29
39	Nanning	0.30	0.18	2.53	0.20	0.13	0.06	0.97	1.36	0.95	0.92	0.0107	1.4272	0.07	-121.92	-33.35
40	Panyu	0.26	0.16	2.29	0.16	0.10	0.06	0.69	1.43	0.93	0.90	0.0137	1.4155	0.07	-96.03	-26.56

41	Shanghai	0.40	0.15	1.93	0.19	0.08	0.11	0.68	1.10	0.84	0.88	0.0142	1.4814	0.07	-106.89	-24.34
42	Shenyang	0.31	0.16	2.23	0.22	0.12	0.10	0.89	1.20	0.90	0.84	0.0253	1.4589	0.14	-144.88	-15.02
43	Tianjin	0.42	0.16	2.26	0.23	0.10	0.13	0.83	1.11	0.86	0.89	0.0134	1.4957	0.07	-108.09	-33.26
44	Urumqi	0.48	0.14	2.14	0.15	0.04	0.10	0.42	0.93	0.75	0.85	0.0192	1.5371	0.05	-70.55	-11.74
45	Xi'an	0.37	0.16	1.85	0.26	0.11	0.15	0.98	0.98	0.82	0.88	0.0150	1.4888	0.10	-132.55	-35.93
46	Yinchuan	0.38	0.14	2.02	0.11	0.04	0.07	0.37	1.12	0.81	0.94	0.0054	1.4930	0.02	-48.67	-21.89
47	Zhengzhou	0.43	0.18	2.22	0.28	0.12	0.16	0.99	1.10	0.86	0.95	0.0045	1.4626	0.04	-101.10	-46.18
48	Shijiazhuang	0.40	0.16	2.28	0.26	0.12	0.14	0.95	1.09	0.87	0.88	0.0154	1.4754	0.09	-125.05	-33.66
49	Wuhan	0.34	0.17	2.22	0.22	0.12	0.10	1.00	1.16	0.91	0.88	0.0196	1.4779	0.11	-171.80	-20.40
50	Zhuzilin	0.27	0.17	2.45	0.15	0.09	0.05	0.66	1.45	0.94	0.96	0.0049	1.4438	0.03	-73.16	-40.65
	Average	0.37	0.16	2.22	0.21	0.10	0.11	0.79	1.15	0.86	0.90	0.0136	1.4695	0.07	-103.28	-30.05

1324 Table 1 (Continued)

1325 ^a Optical parameters at a wavelength of 440 nm.

1326 ^b Angström exponents between 440 and 870 nm.